Agricultural and Forest Meteorology 322 (2022) 109000

Contents lists available at ScienceDirect

Agricultural and Forest Meteorology

journal homepage: www.elsevier.com/locate/agrformet

A sentinel-2-based triangular vegetation index for chlorophyll content estimation

Binxiang Qian [a,b], Huichun Ye [a,c,*], Wenjiang Huang [a,b,c], Qiaoyun Xie [d,*], Yuhao Pan [a,b], Naichen Xing [a], Yu Ren [e], Anting Guo [a], Quanjun Jiao [a,c], Yubin Lan [f]

[a] State Key Laboratory of Remote Sensing Science, Aerospace Information Research Institute, Chinese Academy of Sciences, Beijing 100094, China
[b] University of Chinese Academy of Sciences, Beijing 100049, China
[c] Key Laboratory for Earth Observation of Hainan Province, Sanya 572029, China
[d] School of Life Sciences, Faculty of Science, University of Technology Sydney, NSW 2007, Australia
[e] College of Urban and Environmental Sciences, Peking University, Beijing 100091, China
[f] School of Agricultural Engineering and Food Science, Shandong University of Technology, Zibo 255000, Shandong, China

ARTICLE INFO

Keywords:
Remote sensing
Vegetation
Chlorophyll content retrieval
Sentinel-2 triangular vegetation index (STVI)
Chlorophyll sensitivity

ABSTRACT

Accurate estimation of chlorophyll content is important for diagnosing the physiological and phenological status of vegetation. Establishing the relationship between vegetation indices (VIs) and leaf chlorophyll content using remote sensing is crucial for large-scale earth observation. However, existing VIs for estimating chlorophyll content generally suffer from the saturation effect or depend on specific scenarios, resulting in insufficient estimation accuracy. Based on the physical mechanism of light-vegetation interaction, this study innovatively proposes the absorption triangle and reflectance triangle in the spectral space to construct the chlorophyll-sensitive Sentinel-2 Triangular Vegetation Index (STVI). The STVI uses the Sentinel-2 multispectral instrument (MSI) bands to improve the accuracy of chlorophyll content retrieval by enhancing the relationship with the chlorophyll content and mitigating the saturation effect. Simulated data, measured data, and open data sets were used to test the accuracy and stability of the STVI and 11 classical VIs for retrieving the chlorophyll content using different spectral data types, different winter wheat growth stages, and different vegetation coverages. The results showed that the STVI was more sensitive to the chlorophyll content than the classical VIs and provided the best goodness-of-fit in multiple scenarios. The STVI represents a powerful tool for large-extent chlorophyll content retrieval and a novel approach for scientific research in related fields.

1. Introduction

The leaf chlorophyll content (Chl) is a highly sensitive proxy for external environmental stress (Houborg et al., 2011), photosynthetic capacity (Gitelson et al., 2014, 2006), and the vigor and metabolic activity (Zarco-Tejada et al., 2001) of crops. Chlorophyll reflects the growth status of crops and the material and energy exchange between crops and the outside world (Gitelson and Merzlyak, 1998; Ptushenko et al., 2014; Velichkova and Krezhova, 2019). In remote sensing, the Chl is an important indicator of plant growth status (He et al., 2018; Wu et al., 2008; Zhang et al., 2019). Previous studies have shown that remote sensing plays a unique and essential role in large-scale earth observation by establishing physical mechanisms between the observed signals at the canopy scale and the physicochemical parameters of vegetation on the Earth's surface and deriving empirical statistics (Clevers and Kooistra, 2012; (Daughtry et al., 2000); Feret et al., 2008; Gitelson et al., 2014; (Sims and Gamon, 2002); Wu et al., 2008; Zhang et al., 2019). Vegetation indices (VIs) are widely used in remote sensing to retrieve Chl due to their simplicity, convenience, and high computational efficiency (Croft et al., 2014; Verrelst et al., 2015). However, crop canopy reflectance signals are affected by intrinsic factors, such as biochemical parameters (pigment content, water content, etc.) and biophysical parameters (leaf angle distribution (LAD), leaf area index (LAI), etc.), and external factors, such as atmospheric effects, soil background, illumination geometry, and imaging geometry (Goel, 1988; Jacquemoud et al., 2009; Penuelas and Filella, 1998; Xing et al., 2019; Zhang et al., 2020).

Numerous remote sensing studies were conducted on VIs to reduce

* Corresponding authors.
E-mail addresses: yehc@radi.ac.cn (H. Ye), Qiaoyun.Xie@uts.edu.au (Q. Xie).

https://doi.org/10.1016/j.agrformet.2022.109000
Received 30 November 2021; Received in revised form 2 May 2022; Accepted 8 May 2022
Available online 16 May 2022
0168-1923/© 2022 Elsevier B.V. All rights reserved.

the influence of non-photosynthetic components on Chl retrieval. The normalized difference vegetation index (NDVI) and simple ratio vegetation index (SR) exploit the difference between the high absorption in the red band by chlorophyll in healthy vegetation and the high reflectance in the near-infrared (NIR) band by leaf cells to extract vegetation information (Birth and McVey, 1968; Rouse et al., 1974). However, in high vegetation coverage areas, the absorption in the red band is saturated (Sims and Gamon, 2002), resulting in a nonlinear relationship between most VIs and biochemical parameters, such as Chl. The red edge region is highly sensitive to the Chl (Curran et al., 1990; Li et al., 2017), and the red edge position shifts toward the long wave direction when the crop has a high Chl and exhibits vigorous growth (Curran et al., 1990, 1991; Dash and Curran, 2004; Horler et al., 1983). Therefore, the red edge band (Curran et al., 1991; Horler et al., 1983) has been widely used in chlorophyll-sensitive VIs to improve the nonlinear relationships resulting from the saturation effect. Examples include the red edge chlorophyll index (CIre) (Gitelson et al., 2005), red edge NDVI (NDVIre) (Gitelson and Merzlyak, 1994), normalized difference red edge simple ratio (NDRSR) (Slater and Jackson, 1982), MERIS terrestrial chlorophyll index (MTCI) (Dash and Curran, 2004), red edge simple ratio (RSR) (Gitelson et al., 2005), and the Vogelmann red edge index (VREI1) (Vogelmann et al., 1993). Several studies have shown that the green band is less prone to saturation in areas of high Chl (Buschmann and Nagel, 1993; Datt, 1998, 1999; Gitelson and Merzlyak, 1994, 1996). Therefore, VIs, including the green, red, red edge, and NIR band,s have significantly improved the sensitivity to the Chl and reduced the saturation effect (Gitelson and Merzlyak, 1994; Gitelson et al., 2005; Kim et al., 1994; Vogelmann et al., 1993; Zhang et al., 2020). These indices include the green normalized difference vegetation index (GNDVI) (Gitelson and Merzlyak, 1998), green atmospherically resistant index (GARI) (Gitelson et al., 1996), and modified chlorophyll absorption ratio index (MCARI) (Daughtry et al., 2000). Gitelson et al. used the difference in the reflectance between the blue band and red band to correct the atmospheric effect on the green band (Gitelson et al., 1996) and developed the red edge normalized vegetation index (MRENDVI) (Sims and Gamon, 2002) This index reduced the variability of photosynthetically active radiation caused by the soil background, atmospheric absorption, and other non-photosynthetic components (Gitelson et al., 2020; Wu et al., 2008). Haboudane et al. used soil adjustment factors to compensate for the effects of non-photosynthetic components (e.g., soil background) on vegetation albedo (Huete, 1988; Rondeaux et al., 1996) and established the transformed chlorophyll absorption in reflectance index/optimized soil-adjusted vegetation index (TCARI/OSAVI) (Haboudane et al., 2002; Rondeaux et al., 1996).

Research on VI-based Chl retrieval has achieved great success; however, most indices lack universality and stability in complex application scenarios, such as different remote sensing data sources, plant types, crop growth periods, and vegetation coverage (Gitelson et al., 2021, 2020; Sun et al., 2021; Xing et al., 2019). First, remote sensing data sources based on different platforms affect the applicability of VIs. The observation height of field ASD sensors is generally 1.3 m, and the closer the instrument is to the ground, the purer the pixels are in the field of view. In contrast, spaceborne sensors are hundreds or even thousands of kilometers away from the earth's surface, and the images have a large number of mixed pixels (Xing et al., 2019). Compared with multispectral signals recorded by spaceborne sensors, hyperspectral signals collected by ASD sensors have a narrower bandwidth and more bands, complicating the relationship between multispectral VIs and hyperspectral field measurements. Due to mixed pixels and the differences in spectral and spatial resolutions, the accuracy of Chl inversion based on VIs with hyperspectral and multispectral remote sensing data sources is variable (Dash and Curran, 2004). Second, the biophysical and biochemical parameters of crops vary significantly at different growth stages. These changes in the external morphological structure and internal chemical composition lead to substantial differences in the vegetation canopy spectrum, affecting the general applicability of VIs (Pei et al., 2017; Yuping et al., 2008). For example (Avetisyan and Cvetanova, 2021), the Chl and LAI trend increased and then decreased during the growth period of winter wheat (Yu, 2018). VIs are highly sensitive to changes in the Chl during the rising stage when the individual winter wheat plants are small and the soil background contributes significantly to the canopy spectral reflectance. As the winter wheat plants grow, the contribution of the green leaves to the canopy spectral reflectance increases, but the absorption of incident light by the photosynthetic components becomes saturated, leading to a gradual decrease in the sensitivity of VIs to the Chl. Eventually, the saturation effect increases, making it impossible to use VIs to reflect a high Chl.

The reasons for the low stability and accuracy of Chl retrieval by VIs in complex scenes are two-fold. First, VIs suffer from the saturation effect for a high Chl. Second, the photosynthetically active radiation is variable due to the excessive contribution of non-photosynthetic components (LAI, LAD, soil background) to the spectral reflectance (Gitelson et al., 2020; Wu et al., 2008). Therefore, enhancing the sensitivity of VIs to the Chl while suppressing the effect of the non-photosynthetic components is an effective solution to improve the accuracy and stability of Chl retrieval by VIs in complex scenes (Wu et al., 2008; Zhang et al., 2020).

Past studies have shown that triangular VIs improved the retrieval accuracy of the Chl and attenuated the saturation effect by enhancing the linear relationship between the VIs and the biochemical and biophysical parameters (Broge and Leblanc, 2001; Hunt et al., 2011; Xing et al., 2019). The multispectral instrument (MSI) onboard Sentinel-2 includes 13 spectral bands in the visible, near-infrared, and short-wave infrared regions, including four red edge bands, making it highly suitable for agricultural remote sensing (Clevers et al., 2017; Herrmann et al., 2011; Revill et al., 2019). The Chl retrieval accuracy can be improved substantially by developing a new chlorophyll-sensitive index using these bands. The objectives of this study are (1) to establish a new VI for Chl estimation using Sentinel-2 bands; (2) to estimate the Chl with the proposed VI and validate its accuracy with different datasets; (3) to compare the VI's performance with 11 classical VIs.

2. Materials and methods

2.1. Data acquisition

2.1.1. Data overview

Four datasets were used in this study, including the PROSAIL simulated dataset (PSD21), the publicly available datasets Angers03 (Feret et al., 2011), and two winter wheat field experiment datasets conducted in ShunYi in 2016 (SY16) and in XiaoTangShan in 2019 (XTS19). PSD21 was used for correlation analysis between the VIs and the Chl and sensitivity analysis. Angers03 was used to compare the accuracy of Chl retrieval by VIs using hyperspectral and multispectral data. XTS19 was used to compare the applicability of the VIs to retrieve the Chl in different growth periods of winter wheat, and SY16 was used to compare the applicability of the VIs to retrieve the Chl of winter wheat for different vegetation coverages using Sentinel-2 satellite images.

2.1.2. Field experiment dataset

Study Sites: China is the largest wheat producer globally, with winter wheat production accounting for 98% of the total wheat production in the country (Nie et al., 2019). Two field experiments were conducted on winter wheat. One research site was located in Shunyi District, Beijing (116°31′E to 116°53′E, 40°08′N to 40°14′N), and the other site was located at the Xiaotangshan National Precision Agriculture Demonstration Base, Changping District, Beijing (116°26′E, 40°11′N). Both sites are located in a warm-temperate semi-humid continental monsoon climate region, with an average annual precipitation of 507.7 mm, an average annual temperature of 13.8 °C, and a silt-clay loam soil. The field investigation experiment of winter wheat in Shunyi was carried out

in 2016 (Xing et al., 2019); 24 large fields covering more than several hectares with uniform winter wheat growth were selected as the fixed sampling units, and field measurements were carried out at five main growth stages: tillering stage (April 7), jointing stage (April 20), heading stage (May 3), filling stage (May 18), and milk stage (June 9). The pure pixels of winter wheat could be obtained from Sentinel-2 images because the fields were large enough and the sampling points were in the center of the fields. The winter wheat experiment was conducted in Xiaotangshan in 2019 (Qian et al., 2020). The wheat varieties in the test area were "Lunxuan 167″ with a semi-compact plant type and good grain gluten quality and "Jingdong 18″ with a compact plant type and intermediate grain quality. Field measurements were obtained in 32 treatment plots with a fertilizer gradient in four critical growth periods of winter wheat: jointing stage (April 15), heading stage (April 25), flowering stage (May 10), and filling stage (May 20). The plots were 10 $m \times$ 15 m in size and received a normal water supply. The following fertilizer stress treatments were applied: N0 treatment, no fertilization from green to mature stage; N1 treatment, base fertilizer (Sept 2018) 97.5 kg /hm^2 and jointing stage (April 2019) top fertilizer 97.5 kg/hm^2; N2 treatment, 195 kg/hm^2 basal fertilizer (Sept 2018) and 195 kg/hm^2 topdressing at jointing stage (April 2019); N3 treatment, base fertilizer (Sept 2018) 292.5 kg/hm^2 and jointing stage (April 2019) 292.5 kg /hm^2 topdressing. The plots were too small to obtain Sentinel-2 images synchronically.

Canopy spectral measurement: The winter wheat canopy spectra in the two study areas were measured using an ASD FieldSpec spectroradiometer (Analytical Spectral Devices, Inc., Boulder, CO, USA). The spectral range was 350–2 500 nm with a spectral interval of 1 nm. The spectral data were acquired between 10:30 and 14:00 (Beijing time) under clear and cloudless conditions with low wind. Five 1 × 1 m^2 samples were obtained in each sample plot using a diagonal configuration. The spectrometer with a field of view of 25° was located 1.3 m above the canopy and was oriented vertically downward. Calibration with a standard reference plate was conducted at each sampling point before the measurement. The spectral data measurements were repeated 20 times at each sampling location, and the data of the 5 sample points in the plot were averaged to represent the canopy spectral data of the image pixels in the sample area.

Plant measurements: The LAI was obtained, and fresh leaves were sampled synchronously after the canopy spectral measurement. The LAI was measured with an LAI-2200 plant canopy analyzer (Li-COR Biosciences, Inc., Lincoln, NE, USA). The diagonal observation method was used to measure the LAI at the four corners of the 1 × 1 m^2 sample plot. Measurements were obtained 4–5 times at each point, and the average value represented the LAI of the sample plot. The total Chl consisted of the chlorophyll a (Chla) and chlorophyll *b* (Chlb) contents. The Chl was determined using the following method. The test samples were obtained using a 0.25 cm^2 punch; they were divided into two parts. One part was used to measure the dry weight, and the other was soaked in 95% ethanol solution at 25 ℃ for 48 h until it turned white. Subsequently, the absorbance values of the solutions in the visible light wavelengths of 440, 646, and 665 nm were measured using a UV765PC spectrophotometer (Shanghai Precision Scientific Instrument Co., LTD, Shanghai, China). The Chl was calculated as follows (Ren et al., 2020; Zhou et al., 2017, 2019):

$$\mathrm{Chla(mg/L)} = 12.21 * A_{663} - 2.81 * A_{646} \quad (1)$$

$$\mathrm{Chlb(mg/L)} = 20.13 * A_{646} - 5.03 * A_{663} \quad (2)$$

$$\mathrm{Chl(mg/g)} = [(\mathrm{Chl(mg/L)} + \mathrm{Chl(mg/L)}) * V_s(\mathrm{ml})] / [W_{dry\ leaf}(g) * 1000] \quad (3)$$

$$Chl(\mu g / cm^2) = [Chl(mg/g) * W_{dry\ leaf}(g) * 1000] / L_{area}(cm^2) \quad (4)$$

where A_{646} and A_{663} are the absorbance values of the leaf pigment extraction liquid at 646 nm and 663 nm, respectively; V_S(ml) is the volume of the extraction liquid; $W_{dry\ leaf}$(g) is the leaf dry weight; L_{area} is the leaf area.

Imagery: Sentinel-2A and Sentinel-2B were successfully launched on June 23, 2015 and March 07, 2017 respectively. Multispectral images of the Shunyi pilot area were acquired simultaneously with the field measurements on April 10 and 20, May 3 and 13, and June 9, 2016 by the Sentinel-2A satellite. The atmospherically corrected images were downloaded from Google Earth Engine (GEE) (Gorelick et al., 2017) (https://code.earthengine.google.com/). Spectral bands for multispectral instrument (MSI) onboard Sentinel-2A are shown in Table 1 (https://sentinels.copernicus.eu/web/sentinel/user-guides/sentinel-2-msi/resolutions/radiometric).

2.1.3. Publicly available dataset

In addition to the two field survey data sets obtained in 2016 and 2019, this study also used the Angers03 publicly available datasets (http://opticleaf.ipgp.fr/), which have been widely used in remote sensing studies (Feret et al., 2011; Hosgood et al., 1995; Jin and Wang, 2019). The Angers03 dataset consists of physicochemical parameters and leaf ASD spectral information for 43 plants and was collected by the National Institute for Agricultural Research (INRA), Angers, (France). The Angers03 dataset has missing values and outliers (Feret et al., 2008; Hosgood et al., 1995; Zhou et al., 2019). We used linear regression analysis between the VI data and the Chl to compensate for the small number of anomalous samples that were outside of the 95% confidence interval. Finally, 261 Angers03 samples met the requirements of this study.

2.1.4. Simulated dataset

The PSD21 was generated in this study using the PROSAIL-D model to facilitate sensitivity analysis and determine the regression relationship between the VIs and the Chl. PROSAIL-D (Jacquemoud et al., 2009) is the result of the coupling of the leaf-level radiative transfer model PROSPECT-D (Feret et al., 2008; Jacquemoud and Baret, 1990; Qiu et al., 2018) and the canopy bidirectional reflectance model 4SAIL (Jacquemoud et al., 2009). The models were obtained from http://teledetection.ipgp.jussieu.fr/prosail/. The number of model simulations was 2000, and the parameters settings of the PROSAIL-D model are listed in Table 2. The characteristics of the four datasets are described in Table 3.

2.2. Vegetation indices

2.2.1. Classical vegetation indices selected in this research

In this study, 11 representative VIs widely used in Chl retrieval were

Table 1
Spectral Bands for Multispectral Instrument (MSI) Onboard Sentinel-2A.

Band Number	Central wavelength (nm)	Bandwidth (nm)	Spatial resolution (m)
Band1-Coastal aerosol	442.7	21	60
Band2-Blue	492.4	66	10
Band3-Green	559.8	36	10
Band4-Red	664.6	31	10
Band5-Vegetation Red Edge 1	704.1	15	20
Band6-Vegetation Red Edge 2	740.5	15	20
Band7-Vegetation Red Edge 3	782.8	20	20
Band8-NIR	832.8	106	10
Band8a-Vegetation Red Edge 4	864.7	21	20
Band9-Water vapor	945.1	20	60
Band10-SWIR-Cirrus	1373.5	31	60
Band11-SWIR	1613.7	91	20
Band12-SWIR	2202.4	175	20

Table 2
Parameter settings for PROSAIL-D model used for canopy reflectance modeling.

Model	Parameters	Values[a]
PROSPECT-DB	Leaf chlorophyll content (Chl, $\mu g/cm^2$)	Normal distribution of μ=45, σ=12
	Leaf carotenoid content (LCar, $\mu g/cm^2$)	25% of Chl
	Leaf structure parameter (N)	Normal distribution of μ=1.5, σ=0.15
	Leaf mass per area (LMA, g/cm^2)	0.009
	Equivalent water thickness (EWT, cm)	0.01
	Brown pigments (Cbrown)	0
	Leaf area index (LAI)	Normal distribution of μ=4, σ=1.4
	Leaf angle distribution (LAD)	Spherical
	Soil moisture parameter (Psoil)	Normal distribution of μ=0.5, σ=0.15
4SAIL	Solar zenith angle (SZA, ∘)	30
	View zenith angle (VZA, ∘)	10
	View azimuth angle (VAA, ∘)	90
	Fraction of diffuse incident radiation	0.23
	Hot spot effect	0.01

[a]the normal distribution is used instead of the equidistant distribution to improve the simulation of the random distribution of the parameters, where μ is the mathematical expectation, and σ is the standard deviation of the parameters.

selected and classified into three categories according to the characteristics of the VIs: normalized indices, ratio indices, and multi-band indices. The calculation formulas of the VIs for hyperspectral and multispectral data are listed in Table 4.

2.2.2. The proposed vegetation index

The physical mechanism underlying the proposed vegetation index

The spectral reflectance and emission characteristics of vegetation are determined by chemical and morphological properties (Boochs et al., 1990; Zhao, 2013). The high absorption of visible light by Chl and the scattering of NIR light by the leaf cells can be used to extract vegetation information (Birth and McVey, 1968; Rouse, 1973; Rouse et al., 1974) and estimate the Chl. The MSI onboard Sentinel-2 has 13 high-resolution spectral channels, including 4 red-edge bands, providing the possibility of high-precision Chl retrieval (Clevers et al., 2017; Herrmann et al., 2011; Revil et al., 2019). Triangular VIs attenuate the saturation effect by enhancing the linear relationship between the VIs and the biochemical and biophysical parameters (Broge and Leblanc, 2001; Hunt et al., 2011; Xing et al., 2019). The proposed chlorophyll-sensitive Sentinel-2 Triangular Vegetation Index (STVI) replaces the traditional single band with the area of the triangles whose vertices are the reflectivity of multiple bands as the minimum calculation unit. The STVI exploites the advantage of triangular vegetation index and utilizes the rich information in the red-edge bands of the MSI to improve the sensitivity, attenuate the Chl saturation effect, and enhance the linear relationship with Chl.

The establishment of the absorption triangle and reflection triangle

The PROSPECT model is based on plant leaves and considers reflected, absorbed, and transmitted light, while the PROSAIL model and remote sensors are based on light reflected and absorbed by the vegetation canopy and bare soil. In the spectral space, the part above the vegetation reflectance spectrum obtained from the PROSAIL model is absorbed light, and the part below the reflectance spectrum is reflected light. We propose two triangles. The absorption triangle (AT) is located in the light-absorption region and reflects the light absorption capacity of pigments (especially Chl). The reflection triangle (RT) is located in the reflected light region and represents the light reflection capacity. The triangular vertices are particularly important because first, the area of the AT (S_{AT}) is highly sensitive to a change in the Chl and insensitive to blade structure factors. Second, the area of the RT (S_{RT}) is less sensitive to a change in the Chl than S_{AT} and sensitive to blade structure factors. Thus, there is a strong contrast between the absorption and reflection characteristics. The values of S_{AT} and S_{RT} are similar.

Quantitative sensitivity analysis to determine the triangle vertices

The MSI has four red edge bands with high temporal and spatial resolution, enabling a detailed analysis of the AT and RT vertices. The extended Fourier amplitude sensitivity test (EFAST) (Saltelli et al., 1999; Wang et al., 2013; Xie et al., 2018), a global sensitivity analysis method, is used to filter the bands of the MSI and provide a quantitative basis for triangle vertex selection. The EFAST method combines the advantages of the Sobel method and Fourier amplitude sensitivity test. It is robust, computationally efficient, and requires only a small sample size. The method provides all first effects and the total order effect (Saltelli et al., 1999); the former only considers the contribution of a single factor, whereas the latter considers the interaction between different factors. The sentinel-2 MSI band response function was used to convert the PSD21 hyperspectral curve into a multispectral format, and the EFAST method was used to quantify the sensitivity of the four main parameters (Chl, LAI, N content, and soil moisture (Psoil)) with the highest contribution. The experimental results in Fig. 1 show that the green, RE1, and red bands are most affected by the Chl. The contribution of the three bands to the first effects is 94%, 71%, and 94%, and that of the total effects is 93%, 43%, and 93%, respectively. Thus, they are used as vertices of the AT. The vertices of the RT are selected from the RE2, RE3, NIR, RE4, and B9 because the distance between the two triangle areas should be as small as possible. After several trials, the vertices of the RT were determined from the RE2, RE3, and RE4. The S_{AT} and S_{RT} were calculated as follows based on the multispectral and hyperspectral bands, S_{AT-MSI} and S_{RT-MSI} were multispectral equations (MSI), and S_{AT-MSI} and S_{RT-MSI} were hyperspectral equations:

$$S_{AT-MSI} = 0.5 * [(665-560) * (RE_1 - Green) - (705-560) * (Red - Green)] = 0.5 * [105 * (RE_1 - Green) - 145 * (Red - Green)] \quad (5)$$

$$S_{AT-HS} = 0.5 * [105 * (R_{705} - R_{560}) - 145 * (R_{665} - R_{560})] \quad (6)$$

$$S_{RT-MSI} = 0.5 * [(865-740) * (RE_3 - RE_2) - (783-740) * (RE_4 - RE_2)] = 0.5 * [125 * (RE_3 - RE_2) - 43 * (RE_4 - RE_2)] \quad (7)$$

Table 3
The description of the four data sets.

Data Sets	Biochemical parameters of vegetation						Spectral Data			Multiple growth stages
	Parameters	n	Min	Mean	Max	SD	Leaf Level	Canopy Level	Image data	
Angers03	Chl	261	7.005	35.605	106.718	21.005	√			
SY16	LAI	114	0.960	4.280	8.160	1.670		√	√	√
	Chl		14.080	56.470	101.230	17.360				
PSD21	LAI	2000	0.761	4.016	7.170	1.075		√		
	Chl		8.116	44.879	78.250	11.724				
XTS19	LAI	112	0.479	1.763	3.803	0.769		√		√
	Chl		24.241	57.369	81.731	13.052				

Table 4
Vegetation indices used for chlorophyll content retrieval in this research.

Classification	NO	Name	Hyperspectral equations	Multispectral equations (MSI)[a]
Normalized Vegetation Indices	1	Green Normalized Difference Vegetation Index (GNDVI) (Gitelson and Merzlyak, 1998)	$\frac{(R_{750}-R_{550})}{(R_{750}+R_{550})}$	$\frac{(RE_2-Green)}{(RE_2+Green}$
	2	Red edge NDVI (NDVIre) (Gitelson and Merzlyak, 1994)	$\frac{(R_{750}-R_{705})}{(R_{750}+R_{705})}$	$\frac{(RE_2-RE_1)}{(RE_2+RE_1)}$
	3	Normalized Difference Red edge Simple Ratio (NDRSR) (Gitelson et al., 2005)	$\frac{(R_{872}-R_{712})}{(R_{872}+R_{712})}$	$\frac{(NIR-RE_1)}{(NIR+RE_1)}$
	4	Red Edge Normalized Vegetation Index (MRENDVI) (Sims and Gamon, 2002)	$\frac{(R_{750}-R_{705})}{(R_{750}+R_{705}-2*R_{445})}$	$\frac{(RE_2-RE_1)}{(RE_2+RE_1-2*B1)}$
	5	MERIS Terrestrial Chlorophyll Index (MTCI) (Dash and Curran, 2004)	$\frac{(R_{742}-R_{702})}{(R_{702}+R_{661})}$	$\frac{(RE_2-RE_1)}{(RE_1+Red)}$
Ratio Vegetation Indices	6	Red edge Chlorophyll Index (CIre) (Gitelson et al., 2005)	$\frac{R_{835}}{R_{740}}$-1	$\frac{NIR}{RE_2}$-1
	7	Red edge Simple Ratio (RSR) (Gitelson et al., 2005)	$\frac{R_{872}}{R_{712}}$	$\frac{NIR}{RE_1}$
	8	Vogelmann Red Edge Index (VREI1) (Vogelmann et al., 1993)	$\frac{R_{740}}{R_{720}}$	$\frac{RE_2}{RE_1}$
Multi-band Vegetation Indices	9	Transformed Chlorophyll Absorption in Reflectance Index/Optimized Soil-Adjusted Vegetation Index (CCII=$\frac{TCARI}{OSAVI}$) (Wu et al., 2008)	$\frac{3*[(R_{700}-R_{670})-0.2*(R_{700}-R_{550})*(R_{700}/R_{670})]}{(1+0.16)*(R_{800}-R_{670})/(R_{800}+R_{670}+0.16)}$	$\frac{3*[(RE_1-Red)-0.2*(RE_1-Green)*(RE_1/Red)]}{(1+0.16)*(\mathrm{NIR}-Red)/(\mathrm{NIR}+Red+0.16)}$
	10	Green Atmospherically Resistant Index (GARI) (Gitelson et al., 1996)	$\frac{R_{800}-[R_{550}-\gamma(R_{490}-R_{670})]}{R_{800}+[R_{550}-\gamma(R_{490}-R_{670})]}(\gamma=1.7)$	$\frac{NIR-[Green-\gamma(Blue-Red)]}{NIR+[Green-\gamma(Blue-Red)]}(\gamma=1.7)$
	11	Modified Chlorophyll Absorption Ratio Index (MCARI) (Daughtry et al., 2000)	$[(R_{700}-R_{670})-0.2(R_{700}-R_{550})]\left(\frac{R_{700}}{R_{670}}\right)$	$[(RE_1-Red)-0.2(RE_1-\mathrm{Green})]\left(\frac{RE_1}{Red}\right)$

[a]The multispectral equations are based on the multispectral instrument (MSI) onboard Sentinel-2, which includes 13 spectral bands in the visible, near-infrared, and short-wave infrared regions.

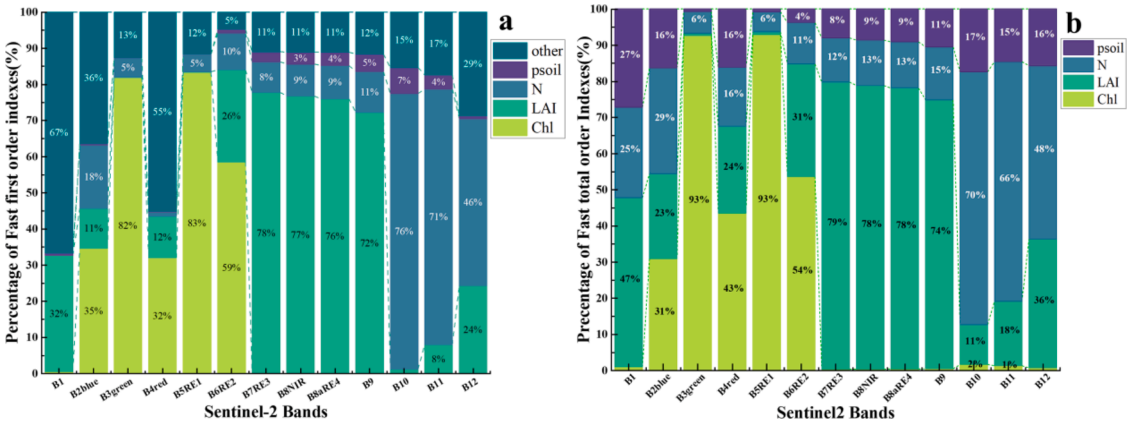


Fig. 1. Global sensitivity analysis of the main parameters of the PROSAIL model.

$$S_{RT-HS} = 0.5 * [125 * (R_{783} - R_{740}) - 43 * (R_{865} - R_{740})] \quad (8)$$

where *Green*, *Red*, RE_1, RE_2, RE_3, and RE_4 are bands 3, 4, 5, 6, 7, and 8A of the MSI, with center wavelengths of 560, 665, 705, 740, 783, and 865 nm, respectively.

The relationship between the Chl and the triangle area

The spectral reflectance of chlorophyll at a Chl of [10:10:80] $\mu g/cm^2$is simulated by the PROSAIL model to determine the relationship between S_{AT}, S_{RT}, and the Chl, as shown in Fig. 2. The following results are obtained: (1) As the Chl increases, the reflectance of the green and red bands decreases, and the position of the red edge moves in the long-wave direction. Thus, the three vertices of the AT converge, and the area of the triangle decreases. This finding indicates that the S_{AT} is negatively correlated with the Chl, but we cannot quantify the absorption capacity of the vegetation pigments in the visible spectrum. (2) As the Chl increases, the reflectance of the NIR band remains constant, the position of the red edge moves towards the long wave direction, the three vertices of the RT diverge, and the area increases. Thus, the S_{RT} is positively correlated with the Chl. (3) S_{AT} is more sensitive than S_{RT} to a change in the Chl, demonstrating the accuracy of using the two triangles.

Establishment of the STVI and its response to the Chl

It is necessary to consider which combination of S_{AT} and S_{RT} can maximize the sensitivity of the STVI to Chl and minimize its sensitivity to blade structure factors. Meanwhile, the ability of triangular vegetation indices to minimize the saturation effect should be exploited to enhance the linear relationship between the STVI and Chl. In this study, the normalized SAT and SRT and their ratios were used in the STVI; they are denoted as $STVI_{Norm}$ (Eq. (9)) and $STVI_{Ratio}$ (Eq. (10)), respectively. The scatter plots between the Chl and the S_{AT}, S_{RT},$STVI_{Norm}$, and $STVI_{Ratio}$ based on the PSD21 are shown in Fig. 3. The following results are obtained: (1) A good exponential relationship is observed between S_{AT} and Chl (R^2=0.917). The relationship is better at a high than a low Chl. However, the linear relationship between S_{RT} and Chl has a much lower R^2 value (R^2=0.677). (2) $STVI_{Norm}$ has a good linear relationship with Chl (R^2=0.892), and the data points are evenly distributed on both sides of the fitting line. $STVI_{Ratio}$ has a good logarithmic relationship with Chl (R^2=0.881), indicating a saturation effect for a low Chl. (3) In

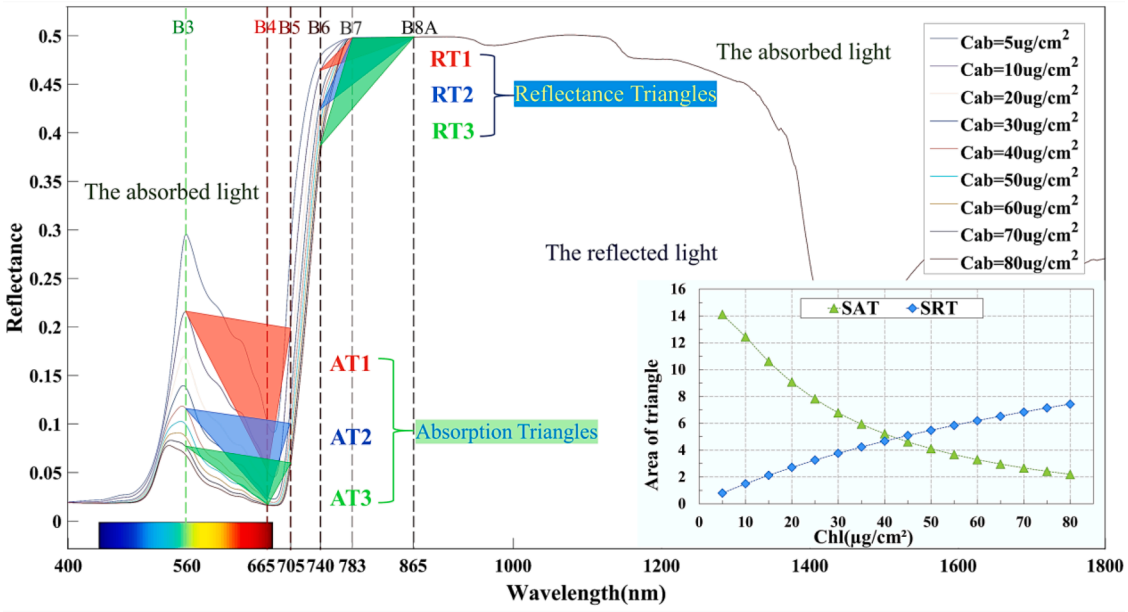


Fig. 2. Schematic diagram of the relationship between S_{AT}, S_{RT}, and the Chl, and the reflectance triangle (RT1, RT2, RT3) and absorption triangle (AT1, AT2, AT3) for Chls of [10,40,70] **ug/cm**^{2}. The plot in the lower right corner depicts the trend of S_{AT} and S_{RT} with the Chl.

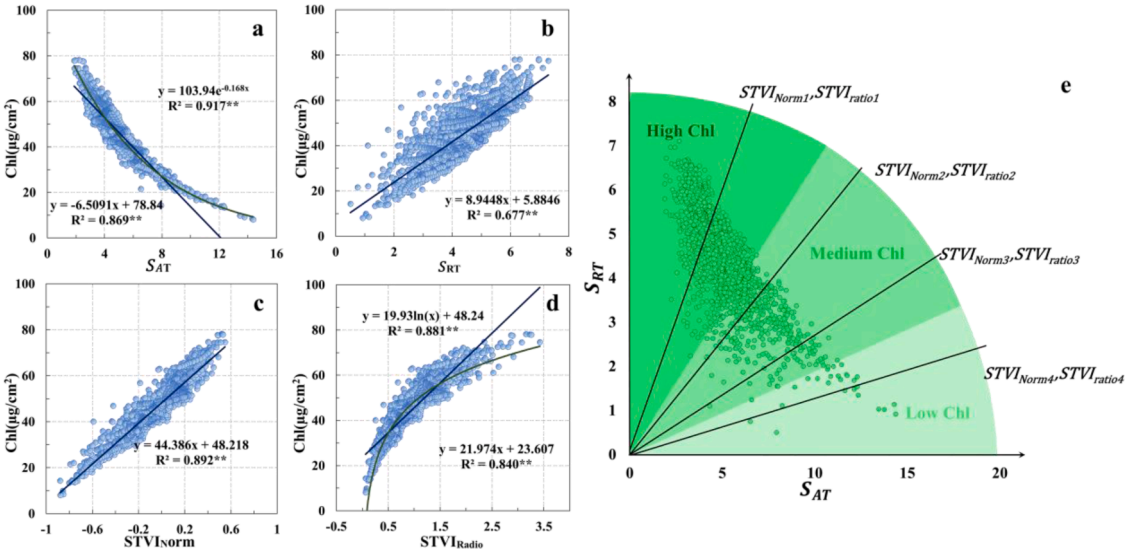


Fig. 3. The scatterplots between Chl and S_{AT}, S_{RT}, $STVI_{Norm}$, and $STVI_{Ratio}$ using the PROSAIL Simulated Dataset (PSD21).

the two-dimensional plot of S_{RT} *vs.* S_{AT}, the higher the slope of the straight line, the higher the Chl is, as shown in Fig. 3e: $STVI_{Norm1}$>$STVI_{Norm2}$>$STVI_{Norm3}$>$STVI_{Norm4}$; $STVI_{Ratio1}$>$STVI_{Ratio2}$>$STVI_{Ratio3}$>$STVI_{Ratio4}$. (4) According to the definition of $STVI_{Norm}$ and $STVI_{Ratio}$, the lines of $STVI_{Norm}$ and $STVI_{Ratio}$ pass through the origin. The $STVI_{Norm}$ is positively correlated with the Chl in the range of [−1,1]. When $STVI_{Norm}$ is close to 0, the Chl is intermediate (close to 40∼50 $\mu g/cm^2$); when $STVI_{Norm}$ tends to 1, the Chl is high, and when $STVI_{Norm}$ approaches −1, the Chl is low. The value range of $STVI_{Ratio}$ is 0∼∞. The $STVI_{Ratio}$ is highly sensitive to the Chl for the points close to the S_{RT} coordinate axis, whereas the $STVI_{Norm}$ values increase with an increase in the slope. Therefore, saturation may occur when $STVI_{Norm}$ is used for the retrieval of the Chl and other vegetation parameters. The $STVI_{Ratio}$ is less affected by saturation; however, noise, the soil background, and other interference factors can affect the $STVI_{Ratio}$.

After comparing the performances of the $STVI_{Norm}$ and $STVI_{Ratio}$, we decided to use the $STVI_{Norm}$, namely, the normalized form of Eq. (9):

$$STVI_{Norm} = \frac{S_{AT} - S_{RT}}{S_{AT} + S_{RT}} \tag{9}$$

$$STVI_{Ratio} = \frac{S_{RT}}{S_{AT}} \tag{10}$$

2.3. Validation strategy

Four datasets were used to compare the accuracy and applicability of Chl retrieval of the STVI and the classical VIs in different scenarios. Each dataset was randomly divided into a training dataset (66.7%) and a validation dataset (33.3%). Based on the distribution characteristics of the scatter plot, the best-fit linear or nonlinear models describing the relationship between the VIs and the Chl were established using the training datasets, and the validation datasets were used to test the model

accuracy. The coefficient of determination (R^2), root mean squared error (RMSE), and standard root mean squared error (NRMSE) of the fitted equation were used as the accuracy evaluation indicesAkhtar et al., 2009; Behdani et al., 2016; Chatterjee and Bandopadhyay, 2012; Peng et al., 2017); they are defined in Eqs. (11)– ((13). It is generally accepted that the model fit is excellent if 0.1 < NRMSE, good if 0.1 ≤ NRMSE < 0.2, average if 0.2 ≤ NRMSE < 0.3, and poor if NRMSE ≥ 0.3 (Peng et al., 2017; Rinaldi et al., 2003). It is assumed that the measured Chl is normally distributed, i.e., the data are clustered around the mean value. The model has high prediction accuracy when the intersection of the 1:1 line and the fitted straight line between the measured and predicted Chl is near the mean value. Since the VIs had different value ranges, they were normalized before the sensitivity analysis (Eq. (14)). The all first effect of the extended Fourier amplitude sensitivity test (EFAST) was used as the quantitative evaluation index of VIs sensitivity to Chl, and the greater the all first effect, the stronger the VIs sensitivity to Chl. At the same time, the standard deviation (SD) of the normalized VIs was used as an auxiliary sensitivity evaluation indicator. The larger the SD, the greater the dispersion of the VIs with Chl variation is, and the stronger the sensitivity of the VI is to the Chl (Zhang et al., 2020), see Eq. (15). The data simulation, preprocessing, and statistical analysis were performed in Matlab R2019a (The Math Works, Inc., Natick, MA, USA).

$$R^2 = 1 - \sum_{i=1}^{n} \frac{(y_i - \widehat{y})^2}{(y_i - \overline{y})^2}, i = 0, 1, \ldots, n \tag{11}$$

$$\mathrm{RMSE}\widehat{y},\ y = \sqrt{\frac{1}{m}\sum_{i=1}^{m}\left(\widehat{y}_i - y_i\right)^2}, i = 0, 1, \ldots, n \tag{12}$$

$$\mathrm{NRMSE}\widehat{y},\ y = \frac{\mathrm{RMSE}\widehat{y},\ y}{\overline{y}} \tag{13}$$

$$\mathrm{Norm_VIs} = \frac{VIs_i - VIs_{min}}{VIs_{max} - VIs_{min}}, i = 0, 1, \ldots, n \tag{14}$$

$$\mathrm{SD} = \sqrt{\frac{1}{m}\sum_{i=1}^{m}(x_i - \overline{x})^2}, i = 0, 1, \ldots, n \tag{15}$$

where y_i, $\widehat{y}_i$, and $\overline{y}$ are the measured value, predicted value, and the average of the measured Chl respectively; VIs_{max} and VIs_{min} are the maximum and minimum values of the VIs, respectively; x_i and $\overline{x}$ are the normalized and mean values of the VIs, respectively.

3. Results

3.1. Comparison of the sensitivity of the VIs to the chlorophyll content using PSD21

Sensitivity is an important indicator to evaluate the response of VIs to a change in the Chl. The higher the sensitivity of the VI to the Chl, the higher the accuracy of the retrieved Chl is. A Chl of [5:5:80] μ /cm^2 was used as the input into PROSAIL and the other parameters were the default values of the model to compare the variation trend of indices with Chl (Fig. 4a-b). The sensitivity of VIs to Chl was quantitatively analyzed using all first effects in the Extended Fourier Amplitude Sensitivity Test (EFAST) (Fig. 4c). The IDEAL line is an auxiliary line that varies linearly with Chl in Fig. 4a-b. In Fig. 4a, Ten VIs, including CCII, GARI, GNDVI, NDRSR, NDVIre, MRENDVI, MCARI, STVI, MTCI, and CIre plotted above the IDEAL line, indicating that they were more sensitive to a low Chl than a high Chl. Two indices (RSR and MTCI) plotted below the IDEAL line, showing that they which more sensitive to a high Chl than a low Chl. The 12 VIs were divided into 2 categories according to the curve's slope. The first group was the VIs sensitive to a low-moderate Chl, which included CCII, GARI, GNDVI, NDRSR, NDVIre, and MRENDVI. However, as the Chl increased, the slope of these VIs decreased, indicating that they became progressively less sensitive to a high Chl content, and saturation occurred. The second category was the VIs that were globally Chl-sensitive, including MCARI, STVI, VREI1, CIre, RSR, and MTCI. They showed a linear relationship with the Chl, indicating no significant saturation effect for the Chl, and the curves were close to the IDEAL line. Among the second group of VIs, MTCI, and RSR showed a gradual increase in the slope with increasing Chl. MCARI, CIre, and VREI1showed a gradual decrease in the slope over the full range of the Chl, i.e., their sensitivity to the Chl gradually decreased with the increasing Chl. Unlike the single trend of the other 11 VIs, the slope of the STVI showed an increasing and decreasing trend and peaked

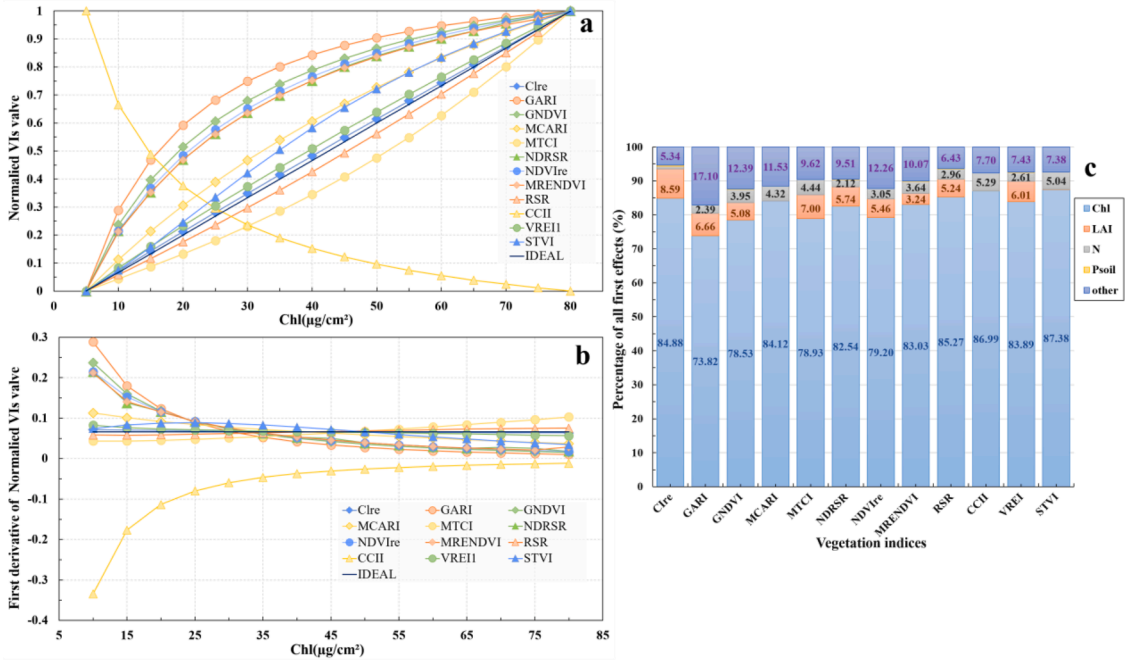


Fig. 4. The relationship between the normalized VI value and the chlorophyll content using the PROSAIL Simulated Dataset (PSD21).

at 25 μg/cm^2 of Chl in Fig. 4b; thus, the STVI was more sensitive to a low-medium Chl than to a high Chl.

Table 5 lists the results of the quantitative accuracy evaluation. The SD of STVI (0.320) was the largest, followed by RSR (0.308), VREI1 (0.306), and CIre (0.306). It was 3.896%~19.850% higher than that of the classical VIs. Based on the SD, the STVI showed the largest dispersion degree to the Chl. In the global sensitivity analysis based on EFAST method, STVI has the largest all first effects on Chl with 0.874, followed by CCII (0.870), RSR (0.853), and CIre (0.849). It was 0.448% ~18.369% higher than that of the classical VIs.

3.2. Correlation between VIs and chlorophyll content using PSD21 and angers03

Leaf spectral reflectance is determined by the biochemical composition of leaves; however, canopy spectral reflectance is related to the internal biochemistry of the leaf and external factors, such as leaf size, leaf density, leaf inclination, soil background, and mixed pixels. Regression relationships were established between the VIs and the Chl using the canopy spectral reflectance from the PSD21 (Fig. 5) and the leaf spectral reflectance from Angers03 (Fig. 6). The relationship between most VIs and the Chl is nonlinear (CCII, GARI, GNDVI, NDRSR, NDVIre, MRENDVI, and MTCI); these VIs showed a saturation effect. Some VIs had a linear relationship with the Chl (CIre, MCARI, RSR, VERI1, and STVI); these VIs had no significant saturation effect over the entire range of the Chl, which was consistent with the results of the sensitivity analysis (Fig. 4). According to the scatterplot characteristics, the VIs were classified into 3 categories. VIs in the first category VIs (CCII, GARI, GNDVI, NDRSR, NDVIre, and MRENDVI) had an exponential relationship with the Chl; thus, they are suitable for low Chl scenarios. The values of the VIs increased slowly, and saturation occurred at a higher Chl (>40 $\mu g/cm^2$). In contrast, the only VI in the second category (MTCI) had a logarithmic relationship with the Chl, making it suitable for high Chl scenarios. At a high Chl, MTCI increased slowly, and saturation occurred at low Chl (<40$\mu g/cm^2$). VIs in the third category (CIre, MCARI, RSR, VERI1, and STVI) had a linear relationship with the Chl and were sensitive to the Chl in the full range of values. These VIs did not exhibit a saturation effect; thus, they are suitable for the full range of Chl. The distribution of the values in the scatterplot was spindle-shaped.

The first group of VIs was normalized difference VIs, except for GARI and CCII, which were multi-band VIs. They generally exhibit saturation effects at a high Chl, although green or red edge bands were used instead of the NIR or red bands. Except for MCARI and STVI, the third type of VIs were ratio VIs, with a combination of NIR and red edge bands or two red edge bands. This finding implies that ratio type VIs may have advantages over other types of VIs for Chl inversion. The STVI (R^2= 0.892) exhibited the best fit among VIs with linear relationships. Its R^2 was 0.450%–13.921% higher than the other VIs. The top three VIs with nonlinear relationships included CCII (R^2 =0.918), MRENDVI (R^2 =0.912), and MTCI (R^2 =0.908). Compared to these three VIs, the STVI was in the 4th position, and its R^2 value was 1.794% to 2.915% lower. In summary, the STVI proved sensitive to the Chl in the entire range and had the best-fit linear relationship with the Chl for canopy spectral reflectance, indicating that it was not prone to saturation.

Next, we established the regression relationship between the VIs and the Chl based on the leaf horizontal spectral reflectance of Angers03, and evaluated the accuracy of the Chl retrieval . The hyperspectral information was converted to multispectral information using the MSI band response function of Sentinel-2 to test the applicability of the VIs to hyperspectral and multispectral data.

Accuracy evaluation of VIs for the retrieval of the leaf-level Chl using hyperspectral and multispectral data

Overall, VIs sensitive to a low Chl showed higher accuracy. Angers03 contained low Chl samples with a mean Chl of 35.605 $\mu g/cm^2$. The results in Fig. 4 show that VIs sensitive to a low-moderate Chl (CCII, GARI, GNDVI, NDRSR, NDVIre, and MRENDVI) were more suitable for the Angers03-based Chl inversion. The modeling results (Table 6) and validation results (Fig. 6) confirm this conjecture. Among the five indices with the best fit in Table 6 and Fig. 6, three were VIs sensitive to a low Chl (NDRSR, NDVIre, and MRENDVI), and two were VIs sensitive to the global Chl (STVI and VERI1). In the tests based on the hyperspectral data, the prediction accuracy results of the top 3 VIs were close, including MRENDVI (modeling R^2=0.957, validation RMSE=4.649 μg/cm^2), NDRSR (modeling R^2=0.956, validation RMSE=4.672 μg/cm^2), and STVI (modeling R^2=0.953, validation RMSE=4.680 μg/cm^2). In the tests based on the multispectral data, the NRMSE of the 12 VIs was in the range of [0.131, 0.206], indicating a good fit. The MRENDVI (R^2=0.961) had the highest accuracy in the modeling set, followed by the STVI (R^2=0.955). The STVI (RMSE=4.581 μg/cm^2) had the best fit in the validation set (Fig. 6l), and its RMSE was lower than that of the other VIs by 1.463%–36.604%.

Comparison of the applicability of VIs for the retrieval of leaf-level Chl using hyperspectral and multispectral data

Overall, the R^2 values of the fitted equation between the VIs and the Chl content were generally higher for multispectral than hyperspectral data. The greater the overlap between the hyperspectral data points (blue) and multispectral data points (brown) in Fig. 6, and the closer the regression line was to the 1:1 line, the more applicable the VI was to both hyperspectral and multispectral data. The STVI was most applicable to both data types, with the smallest slope difference (1.090%) between the regression equations of the hyperspectral and multispectral data. VIs with excellent applicability performance included NDVIre (1.185%), RSR (1.218%), and VREI1 (2.605%); those with good applicability performance were GNDVI (3.797%), GARI (4.272%), NDRSR (4.587%), MRENDVI (5.997%), CCII (9.837%), and MTCI (11.613%); MCARI (23.509%) and CIre (84.726%) showed poor applicability. The reason for the higher accuracy of the MCARI and CIre for multispectral data was that noise signals were filtered out, and the influence of extreme values in the reflectance spectrum on the VI calculation was reduced when the Angers03 hyperspectral data were converted into multispectral data using the Sentinel-2 MSI band response function. In summary, the STVI performed well for both hyperspectral and multispectral data at the leaf level, and MRENDVI and STVI had the two highest prediction accuracies for Chl for hyperspectral and multispectral data, respectively.

3.3. Comparing the applicability of VIs to winter wheat at different growth stages using XTS19

The biophysical and biochemical parameters of crops vary considerably at different growth stages, and changes in the external morphological structure and internal chemical composition lead to large

Table 5
Accuracy evaluation results of the sensitivity of the normalized VIs to the Chl.

	Clre	GARI	GNDVI	MCARI	MTCI	NDRSR	NDVIre	MRENDVI	RSR	CCII	VREI1	STVI
Average	0.510	0.751	0.711	0.588	0.423	0.695	0.695	0.692	0.476	0.239	0.527	0.568
SD	0.306	0.277	0.283	0.304	0.305	0.286	0.286	0.287	0.308	0.267	0.306	0.320
All first effects of Chl	0.849	0.738	0.785	0.841	0.789	0.825	0.792	0.830	0.853	0.870	0.839	0.874
Rank[a]	4	12	11	5	10	8	9	7	3	2	6	1

[a]Rank is a comprehensive evaluation based on the all first effects of Chl.

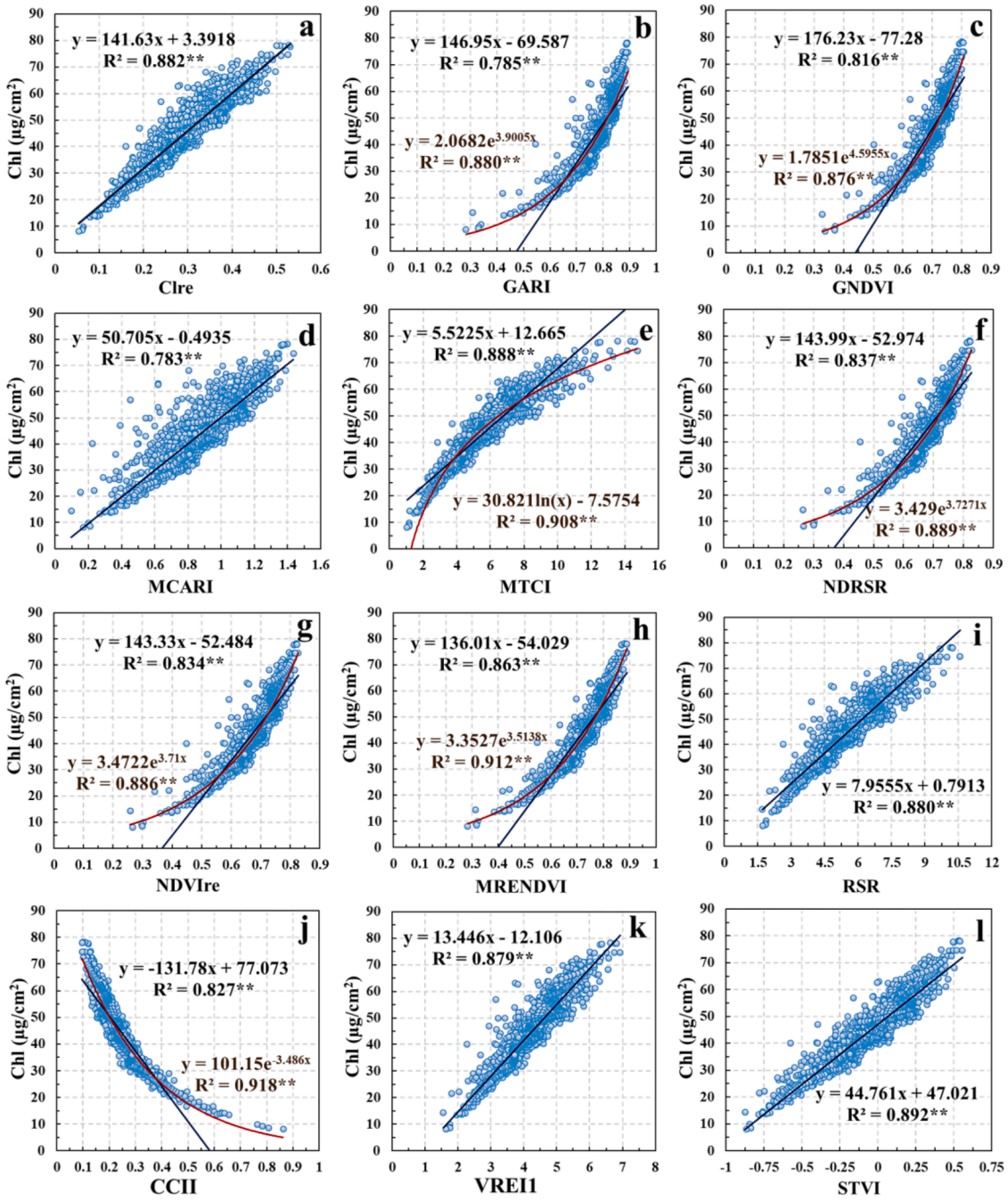


Fig. 5. Relationship between VIs and chlorophyll content at the canopy level using the PROSAIL Simulated Dataset (PSD21), $n = 2000$. Linear equations (blue line) and nonlinear equations (red line) are shown for VIs with nonlinear relationships with the chlorophyll content (* indicates statistical significance at 0.05, ** indicates statistical significance at 0.01).

differences in the vegetation canopy spectrum. The winter wheat experiment in XiaoTangShan in 2019 (XTS19) was used to analyze the applicability of VIs in different crop growth periods. XTS19 contained 112 samples in four growth periods. The Chl increased and then decreased throughout the winter wheat growth stage. The average Chl of the samples was 57.369 μg/cm^2, and those in the jointing stage, heading stage, flowering stage, and filling stage were 50.961, 61.468, 63.139, and 54.523 μg/cm^2, respectively. The regression equations between the VIs and the Chl in different growth periods are listed in Table 7 ($n = 75$), and the validation results of the model are shown in Fig. 7 ($n = 37$). The range of the NRMSE of the 12 VIs was [0.144, 0.173], less than 0.2. The range of the Chl at the intersection point of the fitted line and the 1:1 line was [55, 60] μg/cm^2, which was close to the mean Chl of 57.369 μg/cm^2, demonstrating high model accuracy. The top 5 VIs in terms of accuracy were STVI, MRENDVI, CCII, NDRSR, and NDVIre, and MRENDVI, CCII, NDRSR, and NDVIre were VIs with low-moderate Chl sensitivity (Fig. 4). In addition, the STVI (RMSE=8.381 μg/cm^2) had the highest Chl retrieval accuracy (Fig. 7); its RMSE was 0.957%–16.715% lower than that of the other VIs.

The accuracy of the Chl retrieval models based on single growth period samples of winter wheat using XTS19 is shown in Table 8 Due to the fact that there are few samples of single growth stages in XTS19 (Jointing stage ($n = 29$), Heading stage ($n = 31$), Heading stage ($n = 24$), Filling stage ($n = 28$)), it was impossible to establish an independent regression equation for single growth stages. Therefore, the regression equations established by multi-growth period samples of winter wheat

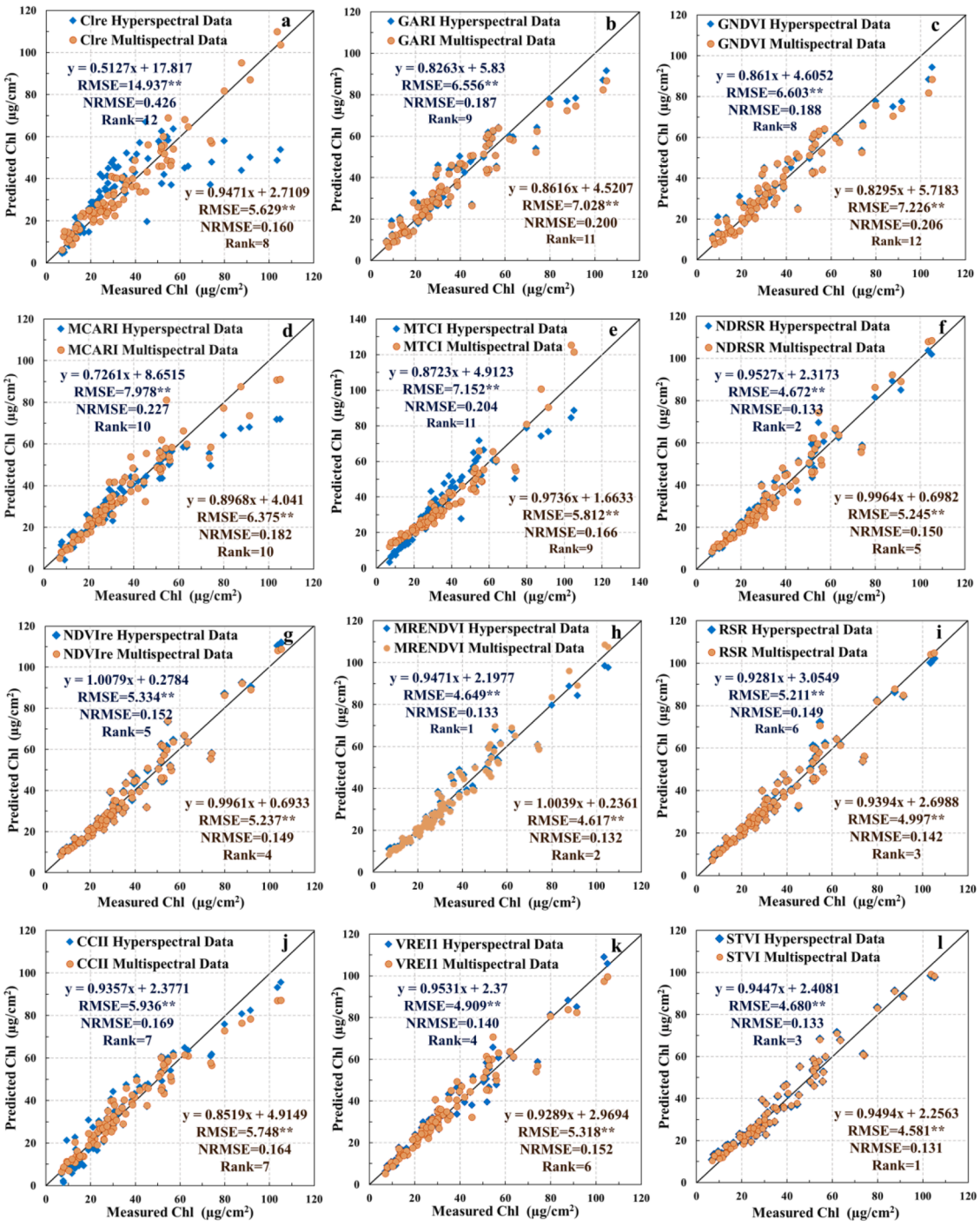


Fig. 6. Calibration results of the retrieval of the leaf-level chlorophyll content by different vegetation indices using Angers03. The scatter plots show the measured and predicted chlorophyll content values in blue for hyperspectral data and in brown for MSI-based multi-band data. The black line is the 1:1 line, $n = 87$ (the rank is based on the RMSE and NRMSE; * indicates the statistical significance at 0.05, ** indicates the statistical significance at 0.01).

in Table 7 were used to verify the Chl retrieval accuracy in the single growing period. The range of the NRMSR for the Chl retrieval in different growth stages was [0.116, 0.197], less than 0.2, indicating excellent model performance. MRENDVI, CCII, and STVI provided the best performances for the combined growth stages. CCII and STVI had higher retrieval accuracies in the jointing stage, heading stage, and flowering stage and lower accuracies in the filling stage than other VIs. In addition, VIs sensitive to growth stage changes included GNDVI and VREI1, both of which performed poorly in the first 3 growth stages and had higher precision in the filling stage, ranking 1st and 2nd, respectively. In summary, MRENDVI, CCII, and STVI exhibited excellent accuracy for winter wheat Chl retrieval. The STVI had the highest accuracy in mixed samples of different growth stages (Fig. 7), while MRENDVI had the highest accuracy in samples of single growth stage (Table 8).

3.4. The applicability of the VIs to different lai levels using sentinel-2 images

Leaf Chl retrieval is highly dependent on the canopy reflectance signal. The Chl is often coupled with biophysical parameters such as the LAI, and it is difficult to remove the effect of the LAI. In this experiment,

Table 6
Fitted equations and R^2 values of the relationship between the VIs and the chlorophyll content using Angers03.

	Hyperspectral data			Multispectral data		
Name	Equation[a]	R^2	Rank	Equation	R^2	Rank
CIre	$y = 7.6206x-7.2687$	0.550**	12	$y = 457x+14.336$	0.928**	9
GARI	$y = 3.2194e^{4.272x}$	0.923**	7	$y = 2.5607e^{4.3901x}$	0.911**	11
GNDVI	$y = 3.0158e^{4.4142x}$	0.907**	10	$y = 2.6829e^{4.5494x}$	0.898**	12
MCARI	$y = 88.047e^{-9.628x}$	0.876**	11	$y = 74.945x+2.8162$	0.928**	8
MTCI	$y = 29.229x-3.3942$	0.909**	9	$y = 11.669x+8.1936$	0.938**	7
NDRSR	$y = 187.76x^2+64.087x+3.9521$	0.956**	2	$y = 5.4069e^{4.2491x}$	0.948**	5
NDVIre	$y = 5.7585e^{4.3067x}$	0.947**	5	$y = 5.3243e^{4.272x}$	0.948**	4
MRENDVI	$y = 183.29x^2-44.604x+13.946$	0.957**	1	$y = 5.2689e^{3.6659x}$	0.961**	1
RSR	$y = 16.756x-13.52$	0.946**	6	$y = 21.389x-19.338$	0.949**	3
$\frac{TCARI}{OSAVI}$ (CCII)	$y = 36.818\ln(x)-0.7287$	0.916**	8	$y = 126.37e^{-2.53x}$	0.927**	10
VREI1	$y = 112.31x-113.01$	0.947**	4	$y = 26.297x-28.133$	0.946**	6
STVI	$y = -44.41x^2+37.905x+93.571$	0.953**	3	$y = -36.737x^2+45.112x+92.264$	0.955**	2

[a]x and y in the equations refer respectively to the VI value and the Chl, $n = 174$ (rank is based on R^2.
*indicates the statistical significance at 0.05.
**indicates the statistical significance at 0.01).

Table 7
Regression equations between VIs and chlorophyll content in all growth periods using XTS19.

NO	Name	Equation[a]	R^2	Rank
1	CIre	$y = 73.646x+28.65$	0.609**	7
2	GARI	$y = 68.375x+7.2426$	0.606**	8
3	GNDVI	$y = 93.198x-5.8464$	0.584**	9
4	MCARI	$y = 24.669x+42.328$	0.359**	12
5	MTCI	$y = 3.2054x+30.321$	0.616**	6
6	NDRSR	$y = 73.955x+7.529$	0.629**	4
7	NDVIre	$y = 73.115x+8.3073$	0.627**	5
8	MRENDVI	$y = 80.262x-2.7332$	0.656**	2
9	RSR	$y = 3.9953x+33.196$	0.521**	10
10	$\frac{TCARI}{OSAVI}$ (CCII)	$y = -153.78x+80.719$	0.631**	3
11	VREI1	$y = 6.8116x+28.556$	0.505**	11
12	STVI	$y = 32.729x+52.498$	0.685**	1

[a]x and y in the equations refer respectively to the VI value and the Chl. ($n = 75$, the rank is based on R^2.
*indicates the statistical significance at 0.05.
**indicates the statistical significance at 0.01).

we used SY16 ground survey data and Sentinel-2 image data to investigate the applicability of the VIs for Chl retrieval for different LAI values scenarios. SY16 consisted of 114 samples obtained in 4 growth stages, and the average Chl was 56.730 μg/cm^2; 64 samples with LAI>4 had an average Chl of 63.718 μg/cm^2; 50 samples with LAI≤4 had an average Chl of 47.780 μg/cm^2. The R^2 of the regression equation between the VIs and the Chl based on the Sentinel-2 image data was in the range of [0.003, 0.389] (Table 9). The accuracies of the models were generally lower than those established based on ground hyperspectral data, which was attributed to the geometry of the MSI and imaging conditions (atmospheric effect, soil background, and mixed pixels). Table 9 shows that the CCII, STVI, NDVIre, MTCI, and CIre performed relatively better for Chl retrieval using image data. The MRENDVI had the worst performance with an R^2 of only 0.003. The slopes of the fitted equations of the measured and predicted Chl in Fig. 8 are in the range of [−0.008, 0.506], less than 1. The range of the Chl for the intersection of the fitting line and the 1:1 line in Fig. 8 is [60, 70] μg/cm^2, which is higher than the mean Chl of 56.730 μg/cm^2, indicating that all 12 VIs overestimated the Chl. More points were above than below the 1:1 line.

The NRMSE of the MRENDVI was 0.354, greater than 0.3, indicating a poor goodness-of-fit (Fig. 8), and the bad and deviating performance of MRENDVI was caused by the difference in spectral and spatial resolutions between Sentinel-2 image data and ground ASD data. Especially the difference between the two in B1 band (443 nm). Whereas the NRMSE of the other 11 VIs were in the range of [0.239,0.286]∈ [0.2,0.3], indicating that their models had moderate goodness-of-fit. For the Chl retrieval models based on satellite images, MTCI (RMSE=12.484 μg/cm^2), STVI (RMSE=12.513 μg/cm^2), and CCII (RMSE=12.716 μg/cm^2) had the best performances. The STVI and MTCI had similar accuracy, with a difference in the RMSE of 0.232%.

In addition, LAI had a great influence on Chl retrieval, accuracy tests were conducted separately for samples with LAI≤4 and LAI>4. It was found that the VI-based Chl retrieval models were sensitive to LAI changes; the results are listed in Table 10. The accuracies of the CCII (RMSE=10.170 μg/cm^2) and STVI (RMSE=10.234 μg/cm^2) were higher for lower LAI values (LAI≤4), whereas the accuracy of MTCI (RMSE=14.455 μg/cm^2) was higher for higher LAI values (LAI>4).

In summary, MTCI and STVI exhibited better performance for Chl retrieval based on satellite image data without separating the LAI into groups. The model accuracy was higher for CCII and STVI when LAI≤4 and for MTCI when LAI>4.

4. Discussion

4.1. Sensitivity analysis results

This study innovatively proposed the AT and RT in the spectral space based on the physical mechanism of light-vegetation interaction and established the Chl-sensitive STVI, normalized VI. To the best of our knowledge, this is the first application of a triangular VIs to retrieve vegetation information related to biochemical composition. Triangular VIs can improve retrieval accuracy by clarifying the relationship between the VI and the physicochemical parameters to mitigate the saturation effect. The experimental results demonstrated that the STVI was sensitive to the Chl in the entire range (Fig. 4), had the best-fit linear relationship with the Chl (Fig. 5), and outperformed classical VIs in several application scenarios (Fig. 6, Fig. 7, Fig. 8). There are two reasons for the high sensitivity of the STVI to the Chl. (1) The STVI is based on the triangular areas (SRT and SAT) rather than single-band reflectance. The latter approach is prone to the saturation effect, whereas the magnitudes of the SRT and SAT depend on the Chl as long as the spectral reflectance corresponding to any of the triangular vertices do not reach the saturation absorption point of the Chl. (2) The S_{AT} is highly sensitive to the Chl and weakly sensitive to blade structure factors, and the S_{RT} has the opposite sensitivity. The combination of the S_{RT} and S_{AT} in the normalized form enhanced the sensitivity of the STVI to the Chl and reduced the interference of the blade structure factors. The sensitivity analysis showed that the CIre, RSR, and VREI1 had a better fit linear relationship with the Chl than the STVI (Table 5). However, unlike the trends of the other 11 VIs, the STVI showed an increase followed by a decrease (based on the all first effects of Chl of the normalized VIs as a

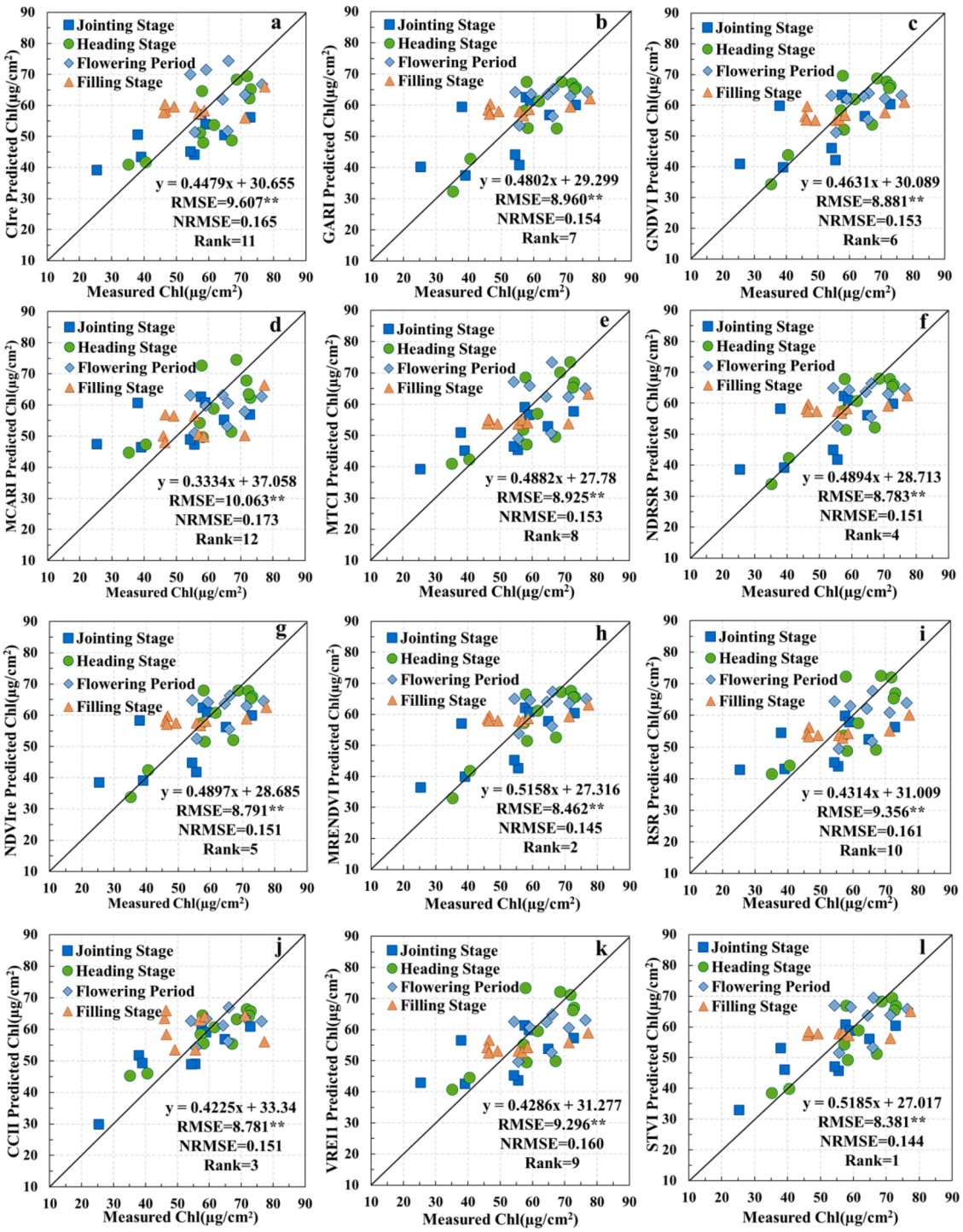


Fig. 7. The chlorophyll content inversion accuracy of the VIs in mixed samples of different winter wheat growth stages. The scatterplots show the measured and predicted Chl. The blue line shows the results for the entire growth period, and the black line is the 1:1 line, $n = 37$. (The rank is based on the RMSE and NRMSE. * indicates the statistical significance at 0.05, ** indicates the statistical significance at 0.01).

sensitivity indicator), indicating that it was more sensitive to the Chl than the other VIs.

4.2. Suitability and accuracy of vegetation indices in different application scenarios

This study analyzed the suitability and accuracy of the proposed STVI and classical VIs for Chl retrieval using simulated datasets, measured datasets, and publicly available datasets in several scenarios: different data types (hyperspectral data, multispectral data, and satellite data), different winter wheat growth stages (jointing stage, heading stage, flowering period, filling stage, and mixed growth stages) and different vegetation coverages (LAI≤4 and LAI>4). The following results were obtained: (1) The STVI did not exhibit significant saturation and had a good fitting linear regression relationship with the canopy-level Chl (Fig. 5), which was supported by the verification test of VIs retrieval of chlorophyll content under different LAI values (Table 10) and different growth periods of winter wheat (Table 8). And the

Table 8
The accuracy of the Chl retrieval models based on single growth period samples of winter wheat.

NO	Name	Jointing stage (n^a=29)				Heading stage (n = 31)				Flowering stage (n = 24)				Filling stage (n = 28)				Summary	
		R^2	RMSE	NRMSE	Rank	R^2	RMSE	NRMSE	Rank	R^2	RMSE	NRMSE	Rank	R^2	RMSE	NRMSE	Rank	Sum	Rank
1	CIre	0.526**	8.307	0.163	5	0.448**	7.830	0.127	8	0.551**	8.829	0.140	11	0.526**	8.574	0.157	10	34	10
2	GARI	0.480**	8.698	0.171	8	0.532**	7.209	0.117	4	0.653**	7.759	0.123	6	0.614**	7.739	0.142	7	25	6
3	GNDVI	0.476**	8.732	0.171	9	0.509**	7.386	0.120	7	0.651**	7.778	0.123	7	0.639**	7.483	0.137	2	25	6
4	MCARI	0.307**	10.042	0.197	12	0.310**	8.754	0.142	12	0.506**	9.256	0.147	12	0.272**	10.624	0.195	12	48	12
5	MTCI	0.543**	8.153	0.16	4	0.441**	7.881	0.128	9	0.568**	8.662	0.137	9	0.630**	7.578	0.139	3	25	6
6	NDRSR	0.511**	8.436	0.166	6	0.528**	7.240	0.118	5	0.665**	7.620	0.121	4	0.621**	7.664	0.141	5	20	4
7	NDVIre	0.511**	8.436	0.166	6	0.528**	7.242	0.118	6	0.665**	7.621	0.121	5	0.619**	7.681	0.141	6	23	5
8	MRENDVI	0.577**	7.852	0.154	3	0.562**	6.976	0.113	1	0.676**	7.495	0.119	2	0.623**	7.646	0.140	4	10	1
9	RSR	0.397**	9.371	0.184	11	0.372**	8.353	0.136	11	0.554**	8.793	0.139	10	0.613**	7.741	0.142	8	40	11
10	$\frac{TCARI}{OSAVI}$(CCII)	0.737**	6.191	0.121	1	0.545**	7.109	0.116	2	0.698**	7.236	0.115	1	0.413**	9.537	0.175	11	15	2
11	VREI1	0.400**	9.344	0.183	10	0.384**	8.274	0.135	10	0.591**	8.424	0.133	8	0.644**	7.426	0.136	1	29	9
12	STVI	0.657**	7.071	0.139	2	0.535**	7.190	0.117	3	0.667**	7.604	0.120	3	0.602**	7.855	0.144	9	17	3

[a]n represents the number of samples collected in each growth period (The rank is based on RMSE and NRMSE.
*indicates the statistical significance at 0.05.
**indicates the statistical significance at 0.01).

Table 9
Regression equations between the VIs and the chlorophyll content using Sentinel-2 images.

NO	Name	Equation[a]	R^2	Rank
1	CIre	$y = 56.706x+39.178$	0.352**	2
2	GARI	$y = 47.183x+27.405$	0.276**	7
3	GNDVI	$y = 57.111x+34.212$	0.196**	10
4	MCARI	$y = 38.663x+46.647$	0.156**	11
5	MTCI	$y = 2.6373x+32.143$	0.389**	1
6	NDRSR	$y = 56.107x+28.208$	0.288**	5
7	NDVIre	$y = 51.647x+32.1$	0.286**	6
8	MRENDVI	$y = 0.1741x+58.748$	0.003	12
9	RSR	$y = 5.2222x+39.493$	0.246**	8
10	$\frac{TCARI}{OSAVI}$ (CCII)	$y = -198.41x+88.305$	0.339**	3
11	VREI1	$y = 9.2172x+34.468$	0.218**	9
12	STVI	$y = 38.5x+48.88$	0.327**	4

[a]x and y in the equations refer respectively to the VI value and the chlorophyll content, n = 76 (the rank is based on R^2.
*indicates the statistical significance at 0.05.
**indicates the statistical significance at 0.01).

responses of the 12 VIs to the Chl were consistent with the sensitivity analysis results (Fig. 4). (2) The differences between the VIs for Chl retrieval using hyperspectral data and multispectral data were relatively small (Table 6, Fig. 6). The difference was attributed to the discrepancy between the central wavelength of the multispectral bands and the wavelengths in the VI equations using hyperspectral data. The MRENDVI and STVI achieved the highest goodness-of-fit for hyperspectral data and multispectral data, respectively. (3) The accuracy of the Chl retrieval models based on single growth period samples and multi-growth period samples of winter wheat differed significantly (Table 7, Table 8, Table 9, Fig. 8). For the multi-growth period samples, the STVI obtained the best goodness-of-fit (Table 7, Fig. 8). For the single growth period samples (Table 8), the MRENDVI provided the best results for all 4 growth stages, while the CCII and STVI had higher retrieval accuracy in the jointing stage, heading stage, and flowering period and lower retrieval accuracy in the filling stage. The proportion of non-photosynthetic components in the canopy spectrum increased because the canopy structure changes significantly during the filling stage as winter wheat seeds mature. (5) The results for different LAI levels showed that CCII and STVI had better performance for low LAI levels or low Chl and were less sensitive to the influence of the soil background (Table 10). On the other hand, CCII and STVI were more sensitive to low-moderate Chl. The MTVI provided the best performance for high vegetation coverage or high Chl. For mixed samples with low, moderate, and high vegetation cover, the MTCI and STVI had the highest accuracy since they are well suited for medium to high-resolution remote sensing imagery.

4.3. Advantages of the STVI

The STVI proved highly suitable for Chl retrieval for different spectral data types, different growth stages, and different vegetation coverages. The innovative concept of replacing a single band with the S_{AT} and S_{RT} as a computing unit provides a new concept for similar research. The suitability of the 12 VIs for Chl retrieval in multiple scenarios was ranked (Table 11). The results indicate that the proposed STVI achieved the best performance based on the accuracy and suitability results in this study, followed by CCII and NDVIre.

4.4. Limitations and implications

This study has the following limitations related to the experimental data and experimental design. First, the STVI includes 3 red edge bands, and there are few satellite sensors with these bands. Although the retrieval model based on the STVI had high accuracy for predicting the

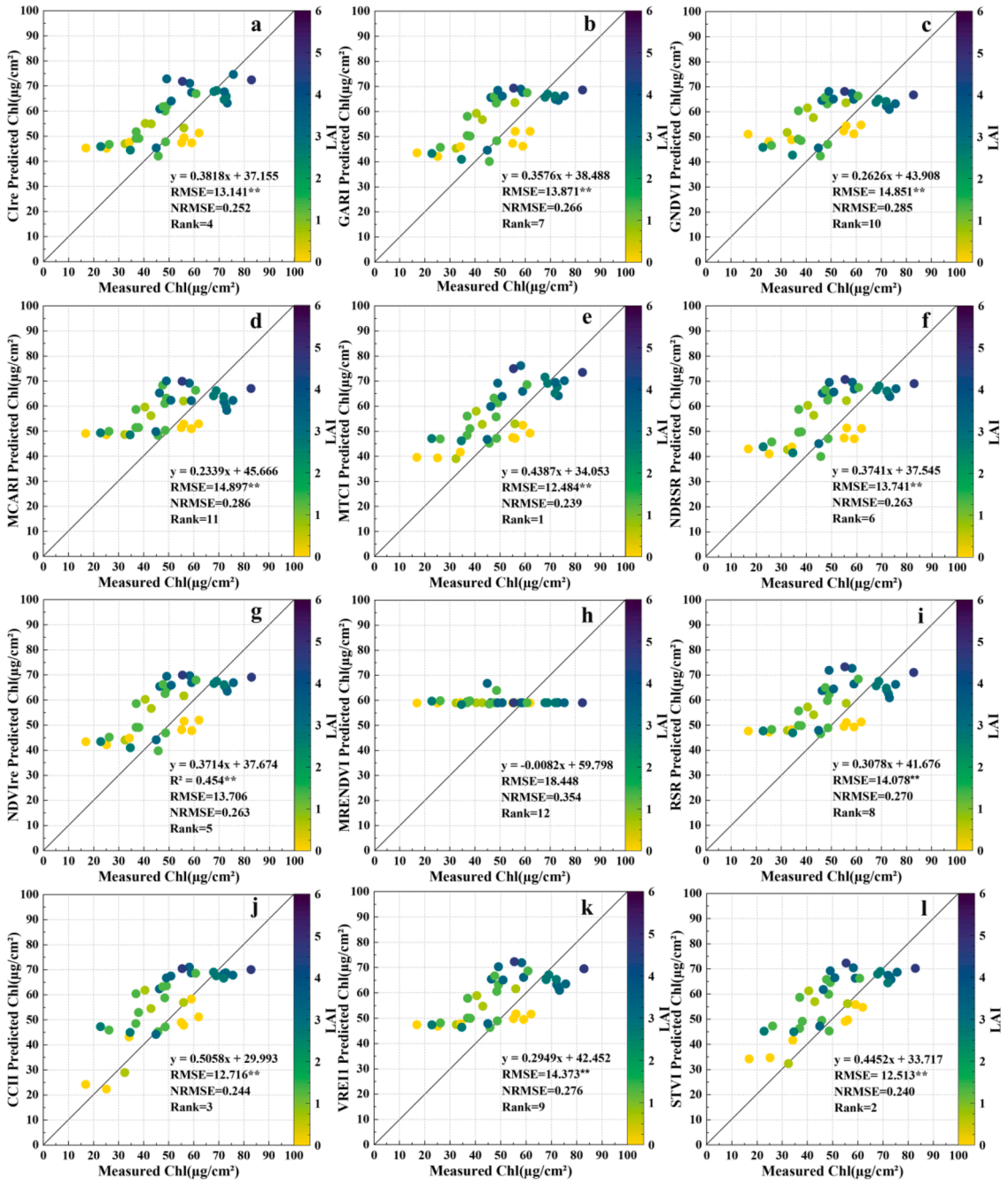


Fig. 8. Accuracies of the vegetation indices for winter wheat chlorophyll content retrieval using Sentinel-2 images. The scatterplots show the measured and predicted chlorophyll content, the blue line is the fitted line, and the black line is the 1:1 line, $n = 38$ (the rank is based on the RMSE and NRMSE. * indicates the statistical significance at 0.05, ** indicates the statistical significance at 0.01).

Chl in various scenarios, only a small number of hyperspectral or multispectral satellites, such as ESA Sentinel-2, China GF-5, and Italy's PRISMA, meet the application requirements. However, the number of satellites with this band configuration will increase in the future, providing potential widespread use of the STVI. Second, the spectral diversity of the field-measured objects used in this study was insufficient; thus, vegetation spectral curves were used to verify the performance of the STVI. In practical applications, vegetation-soil mixed pixels and other field-measured objects, such as water and rocks, should be considered. Third, the Chl retrieval accuracy may be higher for multiple VI combinations than for a single VI. The latest research had utilized random forest machine learning (Shah et al., 2019) and matrix-based VI combination approaches (Xu et al., 2019) for Chl retrieval study, providing less uncertainty than using a single VI. Due to the increasing computational power, machine learning methods in combination with VIs such as the STVI will be used increasingly for large-scale Chl retrieval.

5. Conclusions

This study innovatively proposed the AT and RT in the spectral space based on the physical mechanism of light-vegetation interaction to establish the chlorophyll-sensitive STVI based on the Sentinel-2 MSI bands. The STVI improved the Chl retrieval accuracy by enhancing the relationship with the Chl and mitigating the saturation effect. The accuracy and stability of the STVI and classical VIs were investigated using

Table 10
Comparison of the chlorophyll content retrieval accuracy of the VIs for different LAI values.

NO	Name	LAI≤4 (n = 50)				LAI>4 (n = 64)				Summary	
		R^2	RMSE	NRMSE	Rank	R^2	RMSE	NRMSE	Rank	Sum	Rank
1	CIre	0.213**	10.539	0.221	7	0.321**	15.131	0.237	4	11	5
2	GARI	0.225**	10.461	0.219	5	0.264**	15.758	0.247	7	12	6
3	GNDVI	0.236**	10.384	0.217	4	0.187**	16.566	0.260	9	13	8
4	MCARI	0.174**	10.798	0.226	11	0.125**	17.186	0.270	11	22	11
5	MTCI	0.208**	10.577	0.221	8	0.381**	14.455	0.227	1	9	4
6	NDRSR	0.219**	10.503	0.22	6	0.276**	15.629	0.245	6	12	6
7	NDVIre	0.243**	10.339	0.216	3	0.272**	15.676	0.246	5	8	3
8	MRENDVI	0.002	11.868	0.248	12	0.002	18.354	0.288	12	24	12
9	RSR	0.197**	10.648	0.223	10	0.197**	16.464	0.258	8	18	10
10	$\frac{TCARI}{OSAVI}$(CCII)	0.268**	10.170	0.213	1	0.365**	14.642	0.230	2	3	1
11	VREI1	0.200**	10.629	0.222	9	0.174**	16.695	0.262	10	17	9
12	STVI	0.258**	10.234	0.214	2	0.338**	14.950	0.235	3	5	2

(n = 114, the rank is based on RMSE and NRMSE.
*indicates the statistical significance at 0.05.
**indicates the statistical significance at 0.01).

Table 11
The rankings of the 12 VIs in different tests.

NO	Name	Sensitivity analysis	Fitting		Different data types		Different growth stages		Different vegetation coverages			Sum	Rank[a]
			Linear fitting	Optimization fitting	Hyperspectral data	Multispectral data	Single stage	Multiple stages	LAI≤4	LAI>4	Multiple LAI		
1	CIre	4	3	7	12	8	10	11	7	4	5	71	7
2	GARI	12	11	9	9	11	6	8	5	7	6	84	10
3	GNDVI	11	10	12	8	12	6	6	4	9	8	86	11
4	MCARI	5	12	11	10	10	12	12	11	11	11	105	12
5	MTCI	10	2	3	11	9	6	7	8	1	4	61	6
6	NDRSR	8	7	5	3	5	4	4	6	6	6	54	4
7	NDVIre	9	8	6	5	4	5	5	3	5	3	53	3
8	MRENDVI	7	6	2	1	2	1	2	12	12	12	57	5
9	RSR	3	4	8	6	3	11	10	10	8	10	73	8
10	$\frac{TCARI}{OSAVI}$(CCII)	2	9	1	7	7	2	3	1	2	1	35	2
11	VREI1	6	5	10	4	6	9	9	9	10	9	77	9
12	STVI	1	1	4	2	1	3	1	2	3	2	20	1

[a]Rank is a comprehensive evaluation based on Sum.

different data types, different winter wheat growth periods, and different vegetation coverages with simulated data, measured data, and public datasets. The results showed that the STVI was the most sensitive among all tested VIs to the Chl and did not exhibit a saturation effect. It also provided the best performance under multiple scenarios. Compared with the classical Chl retrieval VIs, the proposed STVI represents a more reliable and powerful VI for large-scale Chl retrieval and a novel concept for establishing new VIs.

CRediT authorship contribution statement

Binxiang Qian: Conceptualization, Formal analysis, Methodology, Software, Writing – original draft, Validation, Visualization. **Huichun Ye:** Methodology, Resources, Supervision, Visualization, Project administration. **Wenjiang Huang:** Conceptualization, Data curation, Resources, Supervision, Funding acquisition. **Qiaoyun Xie:** Formal analysis, Writing – review & editing, Validation. **Yuhao Pan:** Formal analysis, Software, Writing – review & editing, Validation, Visualization. **Naichen Xing:** Investigation, Methodology, Writing – review & editing. **Yu Ren:** Investigation, Methodology, Writing – review & editing. **Anting Guo:** Data curation, Visualization. **Quanjun Jiao:** Validation. **Yubin Lan:** .

Declaration of Competing Interest

The authors declare that they have no known competing financial interests or personal relationships that could have appeared to influence the work reported in this paper.

Acknowledgments

This work was supported by Strategic Priority Research Program of the Chinese Academy of Sciences [grant numbers XDA19080304]; National Natural Science Foundation of China [grant numbers 41871339,41901369, 42071320]; Hainan Provincial High level talent Program of Basic and Applied Basic Research Plan in 2019 of China [grant numbers 2019RC363]; Central Public-interest Scientific Institution BasalResearch Fund [grant numbers Y2021XK24]. The authors would like to thank Xianfeng Zhou, Huiqin Ma, Linyi Liu, Weiping Kong for collecting the field measurement data at Beijing Shunyi District. Also, the authors would like to thank Chang Hong, Ren Yu, Ruan Chao, Jiang Jing, Jin Yu for conducting the field measurements at XiaoTangShan.

References

Akhtar, M., Corzo, G., Van Andel, S., Jonoski, A., 2009. River flow forecasting with artificial neural networks using satellite observed precipitation pre-processed with flow length and travel time information: case study of the Ganges river basin. Hydrol. Earth Syst. Sci. 13, 1607–1618.

Avetisyan, D., Cvetanova, G., 2021. Spectral signature profiles of winter wheat in different growth stages under various environmental conditions, Remote Sensing for Agriculture, Ecosystems, and Hydrology XXIII. SPIE, pp. 268–277.

Behdani, M.A., Al-Ahmadi, M.J., Fallahi, .H..-R., 2016. Biomass partitioning during the life cycle of saffron (Crocus sativus L.) using regression models. J. Crop Sci. Biotechnol. 19, 71–76.
Birth, G.S., McVey, G.R., 1968. Measuring the color of growing turf with a reflectance spectrophotometer1. Agron. J. 60, 640–643.
Boochs, F., Kupfer, G., Dockter, K., Kühbauch, W., 1990. Shape of the red edge as vitality indicator for plants. Remote Sens. (Basel) 11, 1741–1753.
Broge, N.H., Leblanc, E., 2001. Comparing prediction power and stability of broadband and hyperspectral vegetation indices for estimation of green leaf area index and canopy chlorophyll density. Remote Sens. Environ. 76, 156–172.
Buschmann, C., Nagel, E., 1993. In vivo spectroscopy and internal optics of leaves as basis for remote sensing of vegetation. Int. J. Remote Sens. 14, 711–722.
Chatterjee, S., Bandopadhyay, S., 2012. Reliability estimation using a genetic algorithm-based artificial neural network: an application to a load-haul-dump machine. Expert Syst. Appl. 39, 10943–10951.
Clevers, J.G.P.W., Kooistra, L., 2012. Using hyperspectral remote sensing data for retrieving canopy chlorophyll and nitrogen content. IEEE J. Selected Topics Appl. Earth Observ. Remote Sens. 5, 574–583.
Clevers, J.G.P.W., Kooistra, L., Brande, M., 2017. Using sentinel-2 data for retrieving lai and leaf and canopy chlorophyll content of a potato crop. Remote Sens. (Basel) 9, 405.
Croft, H., Chen, J.M., Zhang, Y., 2014. The applicability of empirical vegetation indices for determining leaf chlorophyll content over different leaf and canopy structures. Ecol. Complexity 17, 119–130.
Curran, P.J., Dungan, J.L., Gholz, H.L., 1990. Exploring the relationship between reflectance red edge and chlorophyll content in slash pine. Tree Physiol. 7, 33–48.
Curran, P.J., Dungan, J.L., Macler, B.A., Plummer, S.E., 1991. The effect of a red leaf pigment on the relationship between red edge and chlorophyll concentration. Remote Sens. Environ. 35, 69–76.
Dash, J., Curran, P., 2004. The MERIS terrestrial chlorophyll index.
Datt, B., 1998. Remote sensing of chlorophyll a, chlorophyll *b*, chlorophyll a+b, and total carotenoid content in eucalyptus leaves. Remote Sens. Environ. 66, 111–121.
Datt, B., 1999. A new reflectance index for remote sensing of chlorophyll content in higher plants: tests using eucalyptus leaves. J. Plant Physiol. 154, 30–36.
Feret, J.-.B., François, C., Asner, G.P., Gitelson, A.A., Martin, R.E., Bidel, L.P.R., Ustin, S. L., le Maire, G., Jacquemoud, S., 2008. PROSPECT-4 and 5: advances in the leaf optical properties model separating photosynthetic pigments. Remote Sens. Environ. 112, 3030–3043.
Feret, J.B., François, C., Asner, G.P., Gitelson, A.A., Martin, R.E., Bidel, L., Ustin, S.L., Maire, G.L., Jacquemoud, S., 2011. PROSPECT-4 and 5: advances in the leaf optical properties model separating photosynthetic pigments. Remote Sens. Environ. 112, 3030–3043.
Gitelson, A., Arkebauer, T., Solovchenko, A., Nguy-Robertson, A., Inoue, Y., 2021. An insight into spectral composition of light available for photosynthesis via remotely assessed absorption coefficient at leaf and canopy levels. Photosyn. Res. 1–14.
Gitelson, A., Solovchenko, A., Viña, A., 2020. Foliar absorption coefficient derived from reflectance spectra: a gauge of the efficiency of in situ light-capture by different pigment groups. J. Plant Physiol. 254, 153277.
Gitelson, A.A., Kaufman, Y.J., Merzlyak, M.N., 1996. Use of a green channel in remote sensing of global vegetation from EOS-MODIS. Remote Sens. Environ. 58, 289–298.
Gitelson, A.A., Merzlyak, M.N., 1994. Spectral reflectance changes associated with autumn senescence of aesculus hippocastanum l. and acer platanoides l. leaves. spectral features and relation to chlorophyll estimation. J. Plant Physiol. 143, 286–292.
Gitelson, A.A., Merzlyak, M.N., 1996. Signature Analysis of Leaf Reflectance Spectra: algorithm Development for Remote Sensing of Chlorophyll. J. Plant Physiol. 148, 494–500.
Gitelson, A.A., Merzlyak, M.N., 1998. Remote sensing of chlorophyll concentration in higher plant leaves. Adv. Space Res. 22, 689–692.
Gitelson, A.A., Peng, Y., Arkebauer, T.J., Schepers, J., 2014. Relationships between gross primary production, green LAI, and canopy chlorophyll content in maize: implications for remote sensing of primary production. Remote Sens. Environ. 144, 65–72.
Gitelson, A.A., Viña, A., Ciganda, V., Rundquist, D.C., Arkebauer, T.J., 2005. Remote estimation of canopy chlorophyll content in crops. Geophys Res. Lett. 32.
Gitelson, A.A., Viña, A., Verma, S.B., Rundquist, D.C., Arkebauer, T.J., Keydan, G., Leavitt, B., Ciganda, V., Burba, G.G., Suyker, A.E., 2006. Relationship between gross primary production and chlorophyll content in crops: implications for the synoptic monitoring of vegetation productivity. J. Geophys. Res. 111.
Goel, N.S., 1988. Models of vegetation canopy reflectance and their use in estimation of biophysical parameters from reflectance data. Remote Sens. Reviews 4, 1–212.
Gorelick, N., Hancher, M., Dixon, M., Ilyushchenko, S., Moore, R., 2017. Google Earth Engine: planetary-scale geospatial analysis for everyone. Remote Sens. Environ. 202.
Haboudane, D., Miller, J.R., Tremblay, N., Zarco-Tejada, P.J., Dextraze, L., 2002. Integrated narrow-band vegetation indices for prediction of crop chlorophyll content for application to precision agriculture. Remote Sens. Environ. 81, 416–426.
He, R., Li, H., Qiao, X., Jiang, J., 2018. Using wavelet analysis of hyperspectral remote-sensing data to estimate canopy chlorophyll content of winter wheat under stripe rust stress. Int. J. Remote Sens. 39, 4059–4076.
Herrmann, I., Pimstein, A., Karnieli, A., Cohen, Y., Bonfil, D.J., 2011. LAI assessment of wheat and potato crops by VENμS and Sentinel-2 bands. Remote Sens. Environ. 115, 2141–2151.
Horler, D.N.H., Dockray, M., Barber, J., 1983. The red edge of plant leaf reflectance. Int. J. Remote Sens. 4, 273–288.
Hosgood, B., Jacquemoud, S., Andreoli, G., Verdebout, J., Pedrini, G., Schmuck, G., 1995. Leaf optical properties experiment 93. Joint Res. Center, Eur. Comm., Inst. Remote Sensing ApJacquemoud 75–91.
Houborg, R., Anderson, M.C., Daughtry, C.S.T., Kustas, W.P., Rodell, M., 2011. Using leaf chlorophyll to parameterize light-use-efficiency within a thermal-based carbon, water and energy exchange model. Remote Sens. Environ. 115, 1694–1705.
Huete, A.R., 1988. A soil-adjusted vegetation index (SAVI). Remote Sens Environ 25, 295–309.
Hunt, E.R., Daughtry, C., Eitel, J.U., Long, D.S., 2011. Remote sensing leaf chlorophyll content using a visible band index.
Jacquemoud, S., Baret, F., 1990. PROSPECT: a model of leaf optical properties spectra. Remote Sens. Environ. 34, 75–91.
Jacquemoud, S., Verhoef, W., Baret, F., Bacour, C., Zarco-Tejada, P.J., Asner, G.P., François, C., Ustin, S.L., 2009. PROSPECT+ SAIL models: a review of use for vegetation characterization. Remote Sens. Environ. 113, S56–S66.
Jin, J., Wang, Q., 2019. Selection of informative spectral bands for PLS models to estimate foliar chlorophyll content using hyperspectral reflectance. IEEE Trans. Geosci. Remote Sens. 57, 3064–3072.
Kim, M.S., Daughtry, C., Chappelle, E., McMurtrey, J., Walthall, C., 1994. The use of high spectral resolution bands for estimating absorbed photosynthetically active radiation (A par). In: CNES, Proceedings of 6th International Symposium on Physical Measurements and Signatures In Remote Sensing.
Li, D., Cheng, T., Zhou, K., Zheng, H., Yao, X., Tian, Y., Zhu, Y., Cao, W., 2017. WREP: a wavelet-based technique for extracting the red edge position from reflectance spectra for estimating leaf and canopy chlorophyll contents of cereal crops. ISPRS J. Photogramm. Remote Sens. 129, 103–117.
Nie, H., Qin, T., Yang, H., Chen, J., He, S., Lv, Z., Shen, Z., 2019. Trend analysis of temperature and precipitation extremes during winter wheat growth period in the major winter wheat planting area of China. Atmosphere (Basel) 10, 240.
Pei, H., Feng, H., Li, C., Jin, X., Li, Z., Yang, G., 2017. Remote sensing monitoring of winter wheat growth with UAV based on comprehensive index. Trans. Chinese Soc. Agricult. Eng. 33, 74–82.
Peng, J.-.L., Kim, M.-.J., Jo, M.-.H., Min, D.-.H., Kim, K.-.D., Lee, B.-.H., Kim, B.-.W., Sung, .K..-I., 2017. Accuracy evaluation of the crop-weather yield predictive models of Italian ryegrass and forage rye using cross-validation. J. Crop Sci. Biotechnol. 20, 327–334.
Penuelas, J., Filella, I., 1998. Visible and near-infrared reflectance techniques for diagnosing plant physiological status. Trends Plant Sci. 3, 151–156.
Ptushenko, V.V., Ptushenko, O.S., Tikhonov, A.N., 2014. Chlorophyll fluorescence induction, chlorophyll content, and chromaticity characteristics of leaves as indicators of photosynthetic apparatus senescence in arboreous plants. Biochemistry (Mosc) 79, 260–272.
Qian, B., Huang, W., Huichun, Y., 2020. Inversion of winter wheat chlorophyll contents based on improved algorithms for red edge position. Nongye Gongcheng Xuebao/ Trans. Chinese Soc. Agricult. Eng. 36, 162–170.
Qiu, F., Chen, J.M., Ju, W., Wang, J., Zhang, Q., Fang, M., 2018. Improving the PROSPECT model to consider anisotropic scattering of leaf internal materials and its use for retrieving leaf biomass in fresh leaves. IEEE Trans. Geosci. Remote Sens. 56, 3119–3136.
Ren, Y., Meng, Y., Huang, W., Ye, H., Han, Y., Kong, W., Zhou, X., Cui, B., Xing, N., Guo, A., 2020. Novel vegetation indices for cotton boll opening status estimation using Sentinel-2 data. Remote Sens. (Basel) 12, 1712.
Revill, A., Florence, A., Macarthur, A., Hoad, S.P., Williams, M., 2019. The Value of Sentinel-2 Spectral Bands for the Assessment of Winter Wheat Growth and Development. Remote Sens (Basel) 11, 2050.
Rinaldi, M., Losavio, N., Flagella, Z., 2003. Evaluation and application of the OILCROP–SUN model for sunflower in southern Italy. Agric. Syst. 78, 17–30.
Rondeaux, G., Steven, M., Baret, F., 1996. Optimization of soil-adjusted vegetation indices. Remote Sens. Environ. 55, 95–107.
Rouse, J., Haas, R., Schell, J., Deering, D., Harlan, J., 1974. Monitoring the Vernal Advancements and Retrogradation. Texas A & M University, Texas.
Saltelli, A., Tarantola, S., Chan, .K..-S., 1999. A quantitative model-independent method for global sensitivity analysis of model output. Technometrics 41, 39–56.
Shah, S.H., Angel, Y., Houborg, R., Ali, S., McCabe, M.F., 2019. A random forest machine learning approach for the retrieval of leaf chlorophyll content in wheat. Remote Sens. (Basel) 11, 1–2626.
Slater, P.N., Jackson, R.D., 1982. Atmospheric effects on radiation reflected from soil and vegetation as measured by orbital sensors using various scanning directions. Appl. Opt. 21, 3923–3931.
Sun, Q., Jiao, Q., Qian, X., Liu, L., Liu, X., Dai, H., 2021. Improving the Retrieval of Crop Canopy Chlorophyll Content Using Vegetation Index Combinations. remote sensing 13, 1–20.
Velichkova, K., Krezhova, D., 2019. Extraction of the red edge position from hyperspectral reflectance data for plant stress monitoring.
Verrelst, J., Camps-Valls, G., Muñoz-Marí, J., Rivera, J.P., Veroustraete, F., Clevers, J.G. P.W., Moreno, J., 2015. Optical remote sensing and the retrieval of terrestrial vegetation bio-geophysical properties – A review. ISPRS J. Photogramm. Remote Sens. 108, 273–290.
Vogelmann, J.E., Rock, B.N., Moss, D.M., 1993. Red edge spectral measurements from sugar maple leaves. Int. J. Remote Sens. 14, 1563–1575.
Wang, J., Li, X., Lu, L., Fang, F., 2013. Parameter sensitivity analysis of crop growth models based on the extended fourier amplitude sensitivity test method. Environ. Model. Software 48, 171–182.
Wu, C., Niu, Z., Tang, Q., Huang, W., 2008. Estimating chlorophyll content from hyperspectral vegetation indices: modeling and validation. Agric. For. Meteorol. 148, 1230–1241.

Xie, Q., Dash, J., Huang, W., Peng, D., Qin, Q., Mortimer, H., Casa, R., Pignatti, S., Laneve, G., Pascucci, S., 2018. Vegetation indices combining the red and red-edge spectral information for leaf area index retrieval. IEEE J. Selected Topics Appl. Earth Observ. Remote Sens. 11, 1482–1493.
Xing, N., Huang, W., Xie, Q., Shi, Y., Ye, H., Dong, Y., Wu, M., Sun, G., Jiao, Q., 2019. A transformed triangular vegetation index for estimating winter wheat leaf area index. Remote Sens. (Basel) 12, 1–19.
Xu, M., Liu, R., Chen, J.M., Liu, Y., Shang, R., Ju, W., Wu, C., Huang, W., 2019. Retrieving leaf chlorophyll content using a matrix-based vegetation index combination approach. Remote Sens. Environ. 224, 60–73.
Yu, J.-Y., 2018. Hyper-spectral Estimation Models of Biophysical and Biochemical Parameters of Winter Wheat in Different Stages. North West Agriculture and Forestry University, XiAn,China, p. 96.
Yuping, M., Shili, W., Li, Z., Yingyu, H., Liwei, Z., Yanbo, H., Futang, W., 2008. Monitoring winter wheat growth in North China by combining a crop model and remote sensing data. Int. J. Appl. Earth Obs. Geoinf. 10, 426–437.
Zarco-Tejada, P., Miller, J., Noland, T., Mohammed, G., Sampson, P., 2001. Scaling-up and model inversion methods with narrowband optical indices for chlorophyll content estimation in closed forest canopies with hyperspectral data. Geosci. Remote Sensing, IEEE Trans. 39, 1491–1507.
Zhang, H., Li, J., Liu, Q., Zhao, J., Dong, Y., 2020. A highly chlorophyll-sensitive and LAI-insensitive index based on the red-edge band: CSI, IEEE International Geoscience and Remote Sensing Symposium, pp. 5014–5017.
Zhang, X., He, Y., Wang, C., Xu, F., Li, X., Tan, C., Chen, D., Wang, G., Shi, L., 2019. Estimation of Corn Canopy Chlorophyll Content Using Derivative Spectra in the O2–A Absorption Band. Front Plant Sci 10, 1–13.
zhao, Y., 2013. Principle and Method of Remote Sensing Application Analysis. Science Press, Bei Jing.
Zhou, X., Huang, W., Kong, W., Ye, H., Dong, Y., Casa, R., 2017. Assessment of leaf carotenoids content with a new carotenoid index: development and validation on experimental and model data. Int. J. Appl. Earth Obs. Geoinf. 57, 24–35.
Zhou, X., Huang, W., Zhang, J., Kong, W., Casa, R., Huang, Y., 2019. A novel combined spectral index for estimating the ratio of carotenoid to chlorophyll content to monitor crop physiological and phenological status. Int. J. Appl. Earth Obs. Geoinf. 76, 128–142.
Daughtry, C.S.T., Walthall, C.L., Kim, M.S., de Colstoun, E.B., McMurtrey, J.E., 2000. Estimating corn leaf chlorophyll concentration from leaf and canopy reflectance. Remote Sens. Environ. 74 (2), 229–239.
Sims, D.A., Gamon, J.A., 2002. Relationships between leaf pigment content and spectral reflectance across a wide range of species, leaf structures and developmental stages. Remote Sens. Environ. 81 (2), 337–354.

Further reading

Houborg, R., Boegh, E., 2008. Mapping leaf chlorophyll and leaf area index using inverse and forward canopy reflectance modeling and SPOT reflectance data. Remote Sens. Environ. 112, 186–202.
Liu, L., 2014. Principle and Application of Quantitative Remote Sensing of Vegetation. Science Press, Bei Jing.
Rees, W.G., 2013. Physical Principles of Remote Sensing. Cambridge university press.
Schanda, E., 2012. Physical Fundamentals of Remote Sensing. Springer Science & Business Media.
Smith, H., 1986. The Perception of Light quality, Photomorphogenesis in Plants. Springer, pp. 187–217.
Taiz, L., Zeiger, E., 2002. Plant Physiology.
Tucker, C.J., Garratt, M.W., 1977. Leaf optical system modeled as a stochastic process. Appl. Opt. 16, 635–642.
Xu, X., 2005. Physical Theory of Remote Sensing. Peking University Press, Bei Jing.